APPLICATIONS OF SUBSURFACE RADAR FOR MINE DETECTION

FINAL REPORT

S. ROY, R.S. BERKOWITZ, W.J. GRAHAM AND D. CARLSON

DECEMBER 31, 1990

U. S. ARMY RESEARCH OFFICE

CONTRACT/GRANT NUMBER
DAAL03-87-K-10119

Department of Electrical Engineering
University of Pennsylvania
Philadelphia, PA 19104

MASTER COPY KEEP THIS COPY FOR REPRODUCTION PURPOSES

REPORT DOCUMENTATION PAGE

Form Approved
OMB No. 0704-0188

1. AGENCY USE ONLY *(Leave blank)*	2. REPORT DATE	3. REPORT TYPE AND DATES COVERED
	12/31/90	Final Report: 09/15/87-12/31/90

4. TITLE AND SUBTITLE
Applications of Subsurface Radar for Mine Detection

5. FUNDING NUMBERS

6. AUTHOR(S)
S. Roy, R. S. Berkowitz, W. J. Graham and D. Carlson

7. PERFORMING ORGANIZATION NAME(S) AND ADDRESS(ES)
University of Pennsylvania
Department of Electrical Engineering
Philadelphia, PA 19104

8. PERFORMING ORGANIZATION REPORT NUMBER

9. SPONSORING/MONITORING AGENCY NAME(S) AND ADDRESS(ES)
U. S. Army Research Office
P. O. Box 12211
Research Triangle Park, NC 27709-2211

10. SPONSORING/MONITORING AGENCY REPORT NUMBER

11. SUPPLEMENTARY NOTES
The view, opinions and/or findings contained in this report are those of the author(s) and should not be construed as an official Department of the Army position, policy, or decision, unless so designated by other documentation.

12a. DISTRIBUTION/AVAILABILITY STATEMENT
Approved for public release; distribution unlimited.

12b. DISTRIBUTION CODE

13. ABSTRACT *(Maximum 200 words)*

The principles of a bistatic, forward-looking system for location and identification of isolated, shallow sub-surface objects are described. Experimental data obtained using such a system at L (1.55 MHz and 3.5 MHz) is described, and the results of signal/image processing based on simple, approximate models are presented. The results indicate modest success in isolating target signatures under ideal test-bed conditions, and indicate the need for improved modeling.

14. SUBJECT TERMS
Subsurface Radar; Target Location and Identification

15. NUMBER OF PAGES

16. PRICE CODE

17. SECURITY CLASSIFICATION OF REPORT	18. SECURITY CLASSIFICATION OF THIS PAGE	19. SECURITY CLASSIFICATION OF ABSTRACT	20. LIMITATION OF ABSTRACT
UNCLASSIFIED	UNCLASSIFIED	UNCLASSIFIED	UL

AN, 18581

TABLE OF CONTENTS

1. Introduction

The overall objectives of this project can be summarized as follows:

(i) To obtain experimental justification for a forward-scattering, short pulse synthetic array system concept towards detection and possible imaging of shallow subsurface targets such as anti-tank and anti-personnel mines. Consequently, experimental studies (at L- and S- bands) constituted the primary thrust of this program and are highlighted in the body of the report. Extensive field data was obtained on several test objects as well as mine casings supplied by MERADCOM when buried in an experimental test-bed (constructed under this project) under a variety of conditions at the Valley Forge Research Center's Experimental facility, operated by the Moore School of Electrical Enginnering, University of Pennsylvania. The details of the experimental work are outlined in [1-5]. The promise and the problems of the experimental set-up employed in the study using a bistatic, forward-scattering configuration is described in the section on experimental work.

(ii) Based on the experimental evidence obtained, develop preliminary propagation models and signal processing tools for location, identification and classification of buried objects. The product of this effort include sofware routines for signal/image processing and image display, which are included in the Appendix along with examples of recent images obtained of the mine casings. Other imaging results can be found in [1-5]. The modest success achieved in dry soil conditions indicates the need for improved modeling of wave propagation and interaction at the interfaces, to be used by subsequent enhanced signal processing tools to obtain high-resolution imaging.

2. Experimental Work

2.1 Introduction, General System Considerations

The goal of this part of the program is to study the application of a short pulse, high angular resolution array system, focused in the near-field, to the detection and imaging of shallow sub-surface land mines. The method of implementation is to be synthetic aperture digital beamforming, in which the array element outputs are sequentially sampled, and the beamforming, signal processing, and imaging are performed in the system computer.

The major obstacles to achieving these goals are the varying dielectric constant and conductivity of typical soil types. Land mines are typically only a few centimeters below the soil surface. The relatively high dielectric constant of the soil will cause a large ground surface reflection which may be larger than the return from a target, and both returns may be in the same range bin; even a pulse as short as one nanosecond has a range resolution in sand of 10 cm for backscatter, 20 cm for forward scatter, and probably could not resolve a shallow target from the surface reflection. The finite conductivity of the soil may cause a large attenuation of the signal at higher frequencies, as well as phase variations in the signal return. Also, target dielectric constant may be similar to that of the soil making detection difficult. Finally, the reflections from other subsurface objects such as rocks and roots, may be similar to those from a mine.

The system approach taken may overcome many of these obstacles. Initial experiments were performed using a bistatic forward scattering mode as described in QPR No. 55 [1]. Since the oblique forward scattering from mine geometries is very high compared to backscattering, a much larger target return is obtained in the forward direction. More importantly, the soil reflection coefficient decreases dramatically for oblique forward scattering angles near the Brewster angle as discussed in [1]. Secondly, the use of a high resolution focused array will allow imaging of the mine itself in order to distinguish it from false targets. Initial experiments are being performed at L-band at a frequency of 1550 MHz which will give resolution on the order of the size of a mine. High resolution would be obtained at S-band (e.g. 3500 MHz) so that several resolution cells would exist on the mine.

This section will report on initial results obtained to achieve these goals. Included are the first experimental synthetic aperture array image of a buried mine-like target and experimental results which verify the forward scattering concept.

2.2 Initial Experimental Results

2.2.1 Data Collection and Array Processing Software

The software consists of two primary programs. The first is MINCOLLECT which reads and stores the sampled I and Q channels from the HP 54120T sampling scope for either single event experiments or for each of the 16 element channels in a synthetic aperture array experiment. This program completely automates the experimental data collection since the data is cataloged and can be recalled and plotted on the computer CRT screen at any time. The second program is MINEPROC which is the synthetic aperture array processing program. This program gets the synthetic aperture array data for 16 elements from MINCOLLECT. A data range bin is chosen by the user and a focusing range is also chosen. The program then digitally beamforms in angle for 100 beam positions and the results are scaled and plotted on the CRT as response vs. angle. Both programs have been tested with real data as will be discussed below.

2.2.2 Propagation Experiments

The purpose of these experiments is to determine the reflection and scattering characteristics of soil and targets for various angles of incidence for both backscattering and forward scattering geometries. The experimental setup allows measurement of backscattering for angles of incidence 0° to 90° with the transmit and receive antennas mounted adjacent to each other. For forward scattering measurements, the receive antenna is oriented to the angle of the forward reflected ray, while the transmit antenna is pointed to the desired angle of incidence. The antenna heights and separations are adjusted to insure that they are aimed to a common midpoint on the sand surface.

The experimental procedure is to obtain the level of the incident wave by measuring the direct path signal with the antennas pointed at each other. From knowledge of this level and of the antenna separation, the reflection measurements can be properly normalized to compute reflection coefficients. A normal incidence measurement is then taken at a known height and the voltage reflection coefficient is computed. From this measurement the dielectric constant is determined, and the propagation velocity and wavelength in the sand are computed. This measurement is necessary since the moisture content of the sand varies on a daily basis causing variations in the dielectric constant and signal attenuation.

Four types of propagation measurements have been taken and are discussed below. The target used was a 13" x 17" metal plate. The nominal pulse width is 8 nsec (no range resolution

is needed for these measurements). Vertical polarization was used for all measurements. Horizontal polarization measurements will be performed later for comparison.

a) Interference Measurements (Vertical Incidence)

An interesting phenomenon has been observed when the target is buried at different depths and the reflected signal is measured. The received signal undergoes a cyclic variation in amplitude due to interference between the reflection from the target and the reflection from the sand, as described in Stratton [9]. The depth of maximum signal will depend upon the dielectric constant of the medium. These data are now being analyzed and will be compared with an analytical model. This interference might be utilized to give further information about the target such as depth or composition.

Vertical incidence measurements have also been used to determine dielectric constant. A typical measured value of the voltage reflection coefficient is .37 which gives a dielectric constant of 4.73 and a Brewster angle (angle of incidence for zero surface reflection) of 65.3°.

b) Backscattering Measurements

Preliminary backscattering measurements have been done with the metal plate target at a depth of 2" and an angle of incidence of 45°. The measured voltage reflection coefficient is .108 compared to a measured forward scattering reflection coefficient approaching unity. Although there was no measurable backscattering from the flat sand surface alone, backscattering from a rough surface could easily be as high or higher than that from the target. Additional measurements will be performed at different angles to further characterize backscattering properties.

c) Reflection Coefficient of Sand vs. Angle of Incidence

Because of the utility of the Brewster angle concept for vertical polarization, the voltage reflection coefficient of the sand was measured in the forward scattering setup for varying angle of incidence. As expected its value decreased from about .4 at near vertical incidence to a minimum of .16 as angle increased where upon it again began to increase for angles approaching grazing. The minimum occurs near an angle of 45° rather than the theoretical Brewster angle, probably due to variations in the angle of the sand surface and errors in pointing the antennas. Further experiments will be performed with these errors minimized.

d) Forward Scattering from Buried Target

The previous measurement of surface reflections for varying angle of incidence was repeated with the metal plate buried at a depth of 2". The total reflection coefficient (target plus sand) varies from near unity of vertical incidence to .59 at 60° indicating a much larger forward scattering amplitude than backscattering. When these results are combined with the measured sand surface reflection coefficients, a signal-to-clutter ratio curve can be computed as shown in Figure 3.1. Plotted are the measured values of the forward scattering reflection with the target present normalized by those with the target absent. The peak value occurs at near 45° with a ratio of 17.4 dB. This high level demonstrates the feasibility of detecting buried targets in a forward scattering mode.

e) Focused Array Imaging Experiment

The first experiment to detect and localize a buried target was performed using a 16 element synthetic aperture focused array. The transmit antenna and receiving array were separated by 125" with heights of 36" and pointed at angles of incidence and reflection of 60°. The metal plate was buried at a depth of 2" at the midway point on the sand between the antennas. The single receive array element was moved to 16 sequential positions 4" apart (1/2 wavelength) on a horizontal line perpendicular to the plane of incidence. For each element position, the I and Q channel signals were sampled and stored by the sampling scope and the data were read by the program MINCOLLECT described above. The synthetic aperture array processing program MINEPROC was then used to focus the array at the target range (1.86 m) and to scan the beam to 100 sequential positions in horizontal angle at the target range and compute the response. The resulting image of the metal target is shown in Figure 3.2. The peak response is at the target location and has a width approximately equal to the angular width of the target. The sidelobe response of the array is seen to be very good, on the order of about -13 dB, the theoretical level of a uniform array (no amplitude tapering was used for this initial image although it can easily be incorporated into the program). Sequential images with the array focused at ranges other than the target range show a gradual decrease in peak amplitude.

The relative peak voltage amplitude of the target response is 1261. This is to be compared to the peak response of the image when the target is absent, i.e., of the sand alone. This image is shown in Figure 3.3 where the peak amplitude has decreased to 281. Thus the peak response with the target present is higher than that of the sand alone by 13.8 dB. Therefore the peak response to the sand alone is less than the sidelobe response to the target.

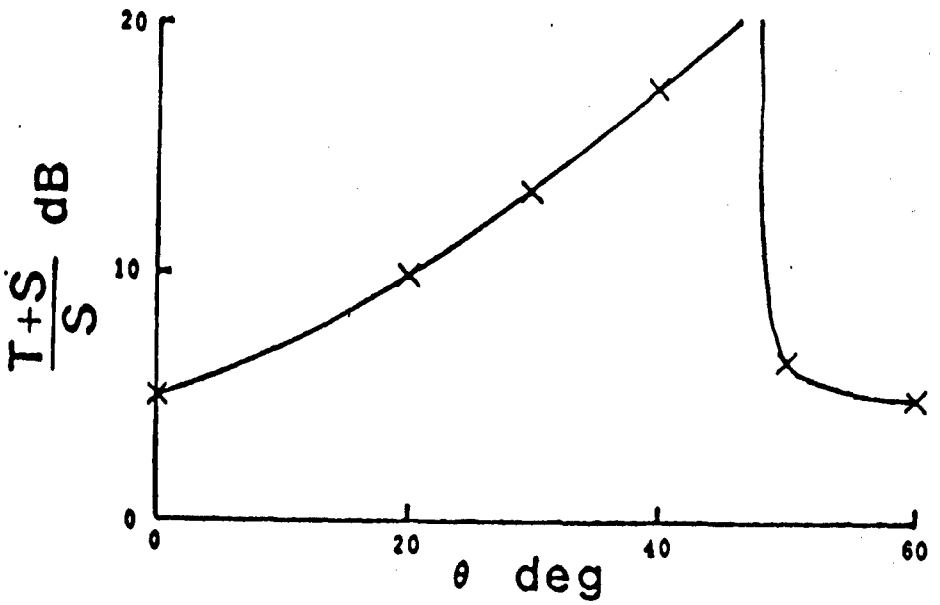

Figure 3.1. Ratio of forward reflection of buried metal target (T) to sand (S) vs. angle of incidence.

These preliminary results indicate a favorable chance for success in imaging of subsurface mines with a focused synthetic aperture array. Additional experimental plans include the use of target of varying dielectric constant including real mine casings, experiments in a moist sand medium, further forward and backscattering experiments for additional angles and ranges, and continuation of array imaging experiments under these conditions. The use of a 1 nsec pulse and the use of S-band hardware can allow even higher resolution imaging.

2.3 Mine Detection System

The system concept proposed is the use of a bistatic radar system operating in the frequency range of L-band to S-band. The lower frequencies are more useful for minimizing attenuation, while the higher frequency range yields more desirable resolution for imaging the mine itself. After a review of the system requirements it was decided to conduct first year experiments with a 4 nsec pulse at L-band initially, despite inadequate range resolution for a shallow subsurface target. The receiver consists of a horizontal line array of equally spaced elements with the image space located in the Fresnel region of its field of view. The transmitting antenna illuminates the ground at an oblique angle, and the receiving array measures the forward scatter from the medium. Each array element then samples and stores the time sequence from each pulse. Digital beamforming is performed in the system computer by focusing and scanning the array in two dimensions (transverse and depth). Imaging in the third dimension (longitudinal) may be assisted by forward motion of the supporting vehicle.

2.3.1 Basic System Features

The initial experiment is performed at 1.5 Ghz using a horn antenna at the transmitter, and dipole/corner-reflector combination antenna at the single receiver. A 500 Mhz scope is used with the receiver to view the envelope of the received waveform provided by an envelope detector. A pulse generator is used as the trigger for a diode switch that generates a 1 nsec pulse modulation of the source frequency. The experiment is performed in a 1-foot deep sandbox of dimensions 8 ft x 16 ft. The experimental setup is based on a 20 Ghz bandwidth HP 54120-T sampling scope. This allows sampling and storage of the entire broadband waveform. The sampling scope interfaces with the HP 9816S computer which can input, store and display the waveform data and perform necessary computations. The data can be transferred to the Moore School laboratory for further processing on the compatible HP 310 or on a VAX system.

2.3.2 A Method of Eliminating Ground Surface Reflections

One of the biggest acknowledged problems in the use of subsurface radar for mine detection is the high amplitude reflection from the air-ground interface. For a normally incident plane wave, the ground-reflected amplitude may be as high as 50% of that of the incident wave, while the reflection from a mine-like target may be much less. This would make detection of the target impossible if it were within the same pulse return as the surface interface. This makes necessary the use of a very short pulse for a shallow target in order to distinguish target response from the surface interface reflection. This imposes severe requirements on the radar

system with the conflicting need for a wide bandwidth, but low frequency to minimize attenuation. Even if this is done, the signal loss from surface reflection may not be affordable.

A potential solution to this problem is proposed; the solution utilizes the polarizing angle or Brewster angle to achieve 100% transmission of incident wave into the earth. If the incident wave is polarized with its electric field parallel to the plane of incidence (corresponding to a vertically polarized antenna), and if the wave is incident at the air-ground Brewster angle, then there will be no surface reflections. The wave transmitted into the ground will, upon reflection from the target (assuming geometical optics reflection), be incident on the ground-air interface at the ground-air Brewster angle, and thus be completely transmitted into the air. Thus, the reflection at both interfaces, air-ground and ground-air, are eliminated with 100% transmission back to the receiver.

A possible scheme for realization of this type of propagation geometry is shown in Figure 3.4. For dry soil with a dielectric constant of 3, the Brewster angle is 60° for the ground-air interface. The transmitting antenna should be rotatable and translatable to achieve this and to adjust for varying Brewster angles.

There are many possible variations of geometry for the receiving array. The most obvious one is with the array perpendicular to the plane of incidence. Both transmit and receive antennas must be vertically polarized. The receiving array should also be capable of rotation and translation in order to optimize the return from various portions of the subsurface area to be imaged.

Another possible geometry of the receiving array is in the plane of incidence. In this case, different array elements would have varying responses to reflections from targets in different regions.

Another advantage of this type of propagation geometry is that the receiving array would be located in the region of forward scattering of the target, a region of very high intensity. An oblique forward-looking monostatic antenna cannot be relied upon because of the low backscattering cross sections of typical targets at oblique angles.

There are many other possibilities as well as problems using this concept for mine detection. A major consideration is the critical angle at which total internal reflection of the target energy occurs at the ground-air interface. This angle is always greater than the Brewster angle, but the angles become closer as the dielectric constant of the ground increases.
Another factor is the finite conductivity of the ground when there is some moisture content. The wavenumber then becomes complex, and reflection and refraction depend upon both dielectric constant and the conductivity of the medium.

The measurements which should be performed in this experiment include:

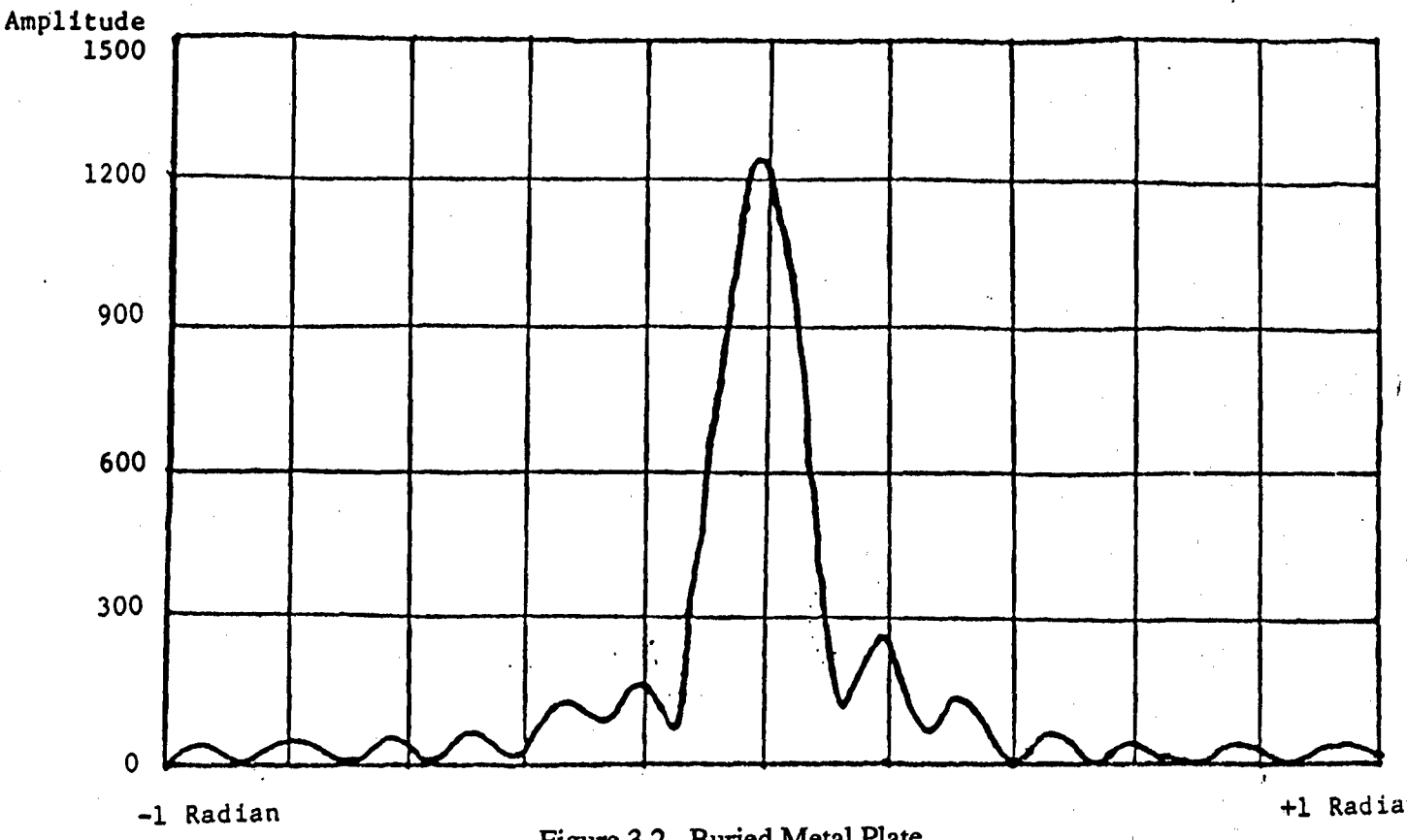

Figure 3.2. Buried Metal Plate

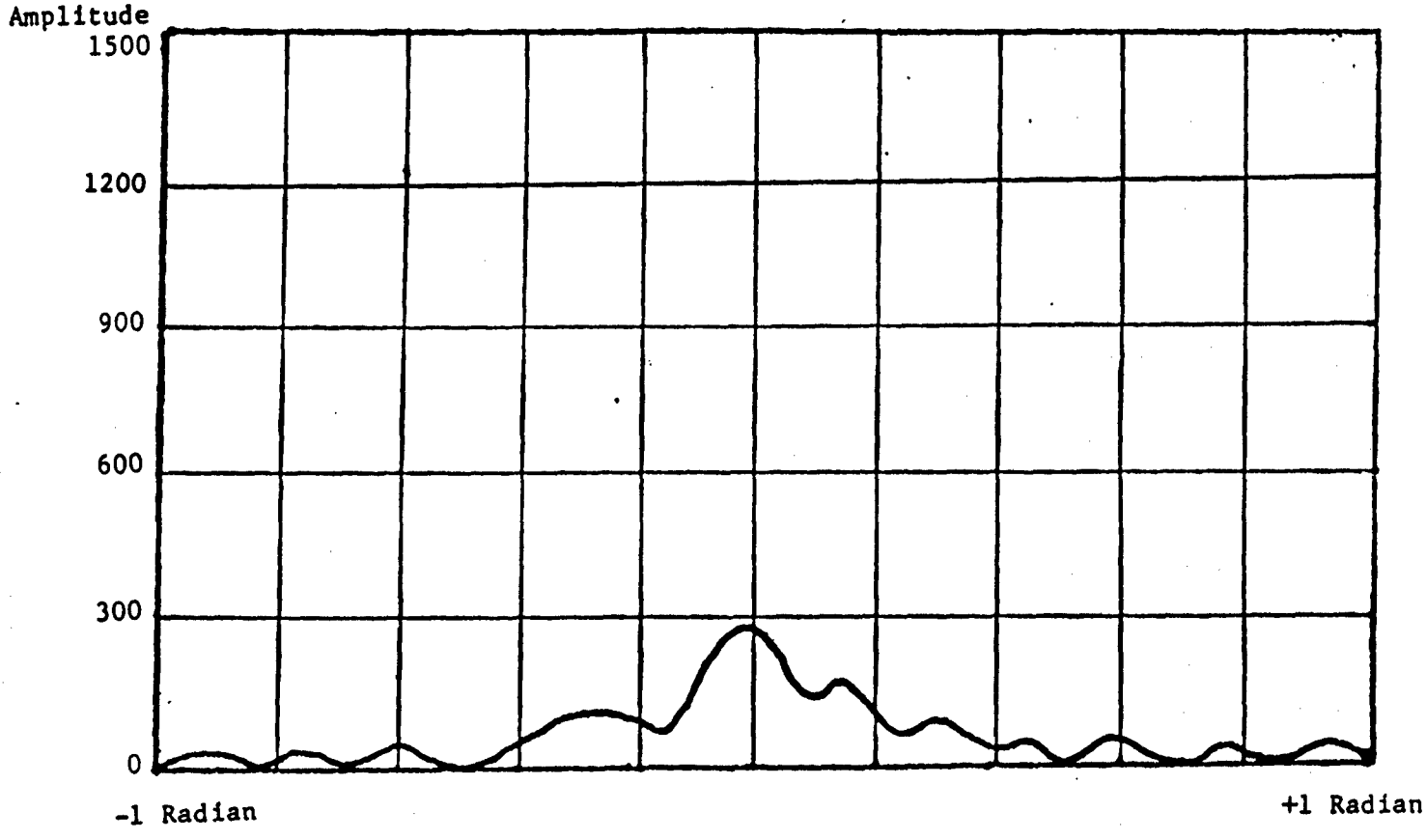

Figure 3.3. Sand Alone

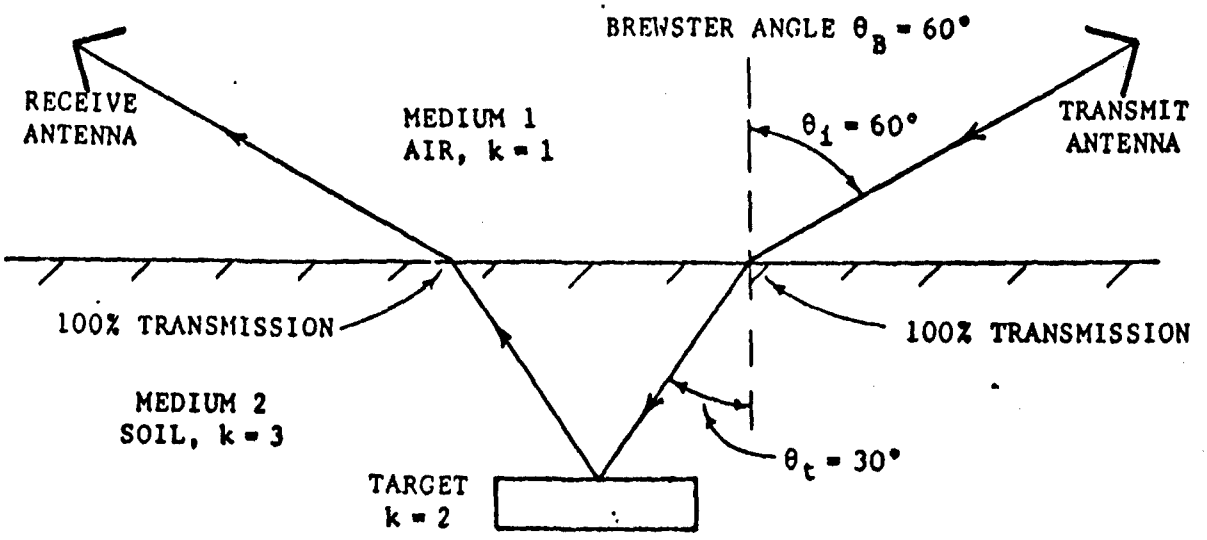

Figure 3.4. Brewster Angle Propagation Geometry

(1) reflection coefficient measurements from air-ground interface for varying angle of incidence, and various soil types and moisture contents;

(2) free-space scattering measurements for various target dielectrics, sizes and shapes for varying angle of incidence;

(3) scattering properties of the targets of (2) when placed in the medium of (1);

The above measurements should be performed for varying depths and horizontal displacements of the targets, as well as varying polarization, transmit antenna directivity, and height of T/R antennas.

2.3.3 Experimental Results

a) System Approach

The goal of this program is to study the application of a short pulse, high angular resolution array system, focused in the near field, to the detection and imaging of shallow subsurface land mines. The method of implementation is to be synthetic aperture digital beamforming, in which the array element outputs are sequentially sampled, and the beamforming, signal processing and imaging are performed in the system computer.

The major obstacles to achieving these goals are the varying dielectric constant and conductivity of typical soil types. Land mines are typically only a few centimeters below the soil surface. The relatively high dielectric constant of the soil will cause a large ground surface reflection which may be larger than the return from a target, and both returns may be in the same range bin; even a pulse as short as one nanosecond has a range resolution in sand of 10 cm for backscatter, 20 cm for forward scatter, and probably could not resolve a shallow target from the surface reflection. The finite conductivity of the soil may cause a large attenuation of the signal for high frequencies, as well as phase variations in the signal return. Also, target dielectric constant may be similar to that of the soil making detection difficult. Finally, the reflections from other subsurface objects such as rocks and roots, may be similar to those from a mine.

The system approach taken overcomes many of these obstacles. Initial experiments were performed using a bistatic forward scattering mode as described in Valley Forge Research Center Quarterly Progress Report No. 55 [1]. Since the oblique forward scattering from mine geometries is very high compared to backscattering, a much larger target return was obtained in forward direction. More importantly, the soil reflection coefficient decreases dramatically for oblique forward scattering angles near the Brewster angle as discussed in [1]. Secondly, the use of a high resolution focused array will allow imaging of the mine itself in order to distinguish it from false targets. Initial experiments were performed at L-band at a frequency of

1550 MHz, which gives resolution on the order of the size of a mine. Higher resolution would be obtained at S-band (e.g., 3.5 GHz) so that several resolution cells would exist on the mine.

This section reports on the initial results obtained to achieve these goals. Included are the first experimental synthetic aperture array image of a buried mine-like target and experimental results which verify the forward scattering concept.

b) Data Collection and Array Processing Software

The software consists of two primary programs. The first is MINCOLLECT which reads and stores the sampled I and Q channels from the HP 54120T sampling scope for either single event experiments or for each of the 16-element channels in a synthetic aperture array experiment. This program completely automates the experimental data collection since the data is catalogued and can be recalled and plotted on the computer CRT screen at any time. The second program is MINEPROC which is the synthetic aperture array processing program. This program gets the synthetic aperture array data for 16 elements form MINCOLLECT. A data range bin is chosen by the user and a focusing range is also chosen. The program then digitally beamforms in angle for 100 beam positions and the results are scaled and plotted on the CRT as response vs. angle. Both programs have been tested with the real data as will be discussed below.

c) Propagation Experiments

The purpose of these experiments has been to determine the reflection and scattering characteristics of soil and targets for various angles of incidence for both backscattering and forward scattering geometries. The experimental setup allows measurement of backscattering for angles of incidence 0° to 90° with the transmit and receive antennas mounted adjacent to each other. For forward scattering measurements, the receive antenna is oriented to the angle of the forward reflected ray, while the transmit antenna is pointed to the desired angle of incidence. The antenna heights and separations are adjusted to insure that they are aimed to a common midpoint on the sand surface.

The experimental procedure is to obtain the level of the incident wave by measuring the direct path signal with the antennas pointed at each other. From knowledge of this level and of the antenna separation, the reflection measurements can be properly normalized to compute reflection coefficients. A normal incidence measurement is then taken at a known height and the voltage reflection coefficient is computed. From this measurement the dielectric constant is determined, and the propagation velocity and wavelength in the sand are computed. This measurement is necessary since the moisture content of the sand varies on a daily basis causing variations in the dielectric constant and signal attenuation.

Four types of propagation measurements have been taken and are discussed below. The target used was a 13" x 17" metal plate. The nominal pulse width is 8 nsec (no range resolution is needed for these measurements). Vertical polarization was used for all measurements. Horizontal polarization measurements will be performed later for comparison.

d) Interference Measurements (Vertical Incidence)

An interesting phenomenon has been observed when the target is buried at different depths and the reflected signal is measured. The received signal undergoes a cyclic variation in amplitude due to interference between the reflection from the target and the reflection from the sand, as described in Stratton [9]. The depth of maximum signal will depend upon the dielectric constant of the medium.

Vertical incidence measurements have also been used to determine dielectric constant. A typical measured value of the voltage reflection coefficient is .37 which gives a dielectric constant of 4.73 and a Brewster angle (angle of incidence for zero surface reflection) of 65.3°.

e) Backscattering Measurements

Preliminary backscattering measurements have been done with the metal plate target at a depth of 2" and an angle of incidence of 45°. The measured voltage reflection coefficient is .108 compared to a measured forward scattering reflection coefficient approaching unity. Although there was no measurable backscattering from the flat sand surface alone, backscattering from a rough surface could easily be as high or higher than that from the target.

f) Reflection Coefficient of Sand vs. Angle of Incidence

Because of the utility of the Brewster angle concept for vertical polarization, the voltage reflection coefficient of the sand was measured in the forward scattering setup for varying angle of incidence. As expected its value decreased from about 0.4 at near vertical incidence to a minimum of 0.16 as angle increased whereupon it again began to increase for angles approaching grazing. The minimum occurs near an angle of 45° rather than the theoretical Brewster angle, probably due to variations in the angle of the sand surface and errors in pointing the antennas.

g) Forward Scattering from Buried Target

The previous measurement of surface reflections for varying angle of incidence was repeated with the metal plate buried at a depth of 2". The total reflection coefficient (target plus sand) varies from near unity at vertical incidence to 0.59 at 60° indicating a much larger forward scattering amplitude than backscattering. When these results are combined with the measured

sand surface reflection coefficients, a signal-to-clutter ratio curve can be computed as shown in Figure 3.5. Plotted are the measured values of the forward scattering reflection with the target present normalized by those with the target absent. The peak value occurs at near 45° with a ratio of 17.4 dB. This high level demonstrates the feasibility of detecting buried targets in a forward scattering mode.

h) Focused Array Imaging Experiments

The first experiment to detect and localize a buried target was performed using a 16-element synthetic aperture focused array. The transmit antenna and receiving array were separated by 125" with heights of 36" and pointed at angles of incidence and reflection of 60°. The metal plate was buried at a depth of 2" at the midway point on the sand between the antennas. The single receive array element was moved to 16 sequential position 4" apart (1/2 wavelength) on a horizontal line perpendicular to the plane of incidence. For each element positions, the I and Q channel signals were sampled and stored by the sampling scope and the data were read by the program MINCOLLECT described above. The synthetic aperture array processing program MINEPROC was then used to focus the array at the target range (1.86 m) and to scan the beam to 100 sequential positions in horizontal angle at the target range and compute the response. The resulting image of the metal target is shown in Figure 3.6. The peak response is at the target location and has a width approximately equal to the angular width of the target. The sidelobe response of the array is seen to be very good, on the order of about -13 dB, the theoretical level of a uniform array (no amplitude tapering was used for this initial image although it can easily be incorporated into the program). Sequential images with the array focused at ranges other than the target range show a gradual decrease in peak amplitude.

The relative peak voltage amplitude of the target response is 1261. This is to be compared to the peak response of the image when the target is absent, i.e., of the sand alone. This image is shown in Figure 3.7 where the peak amplitude has decreased to 281. Thus the peak response with the target present is higher than that of the sand alone by 13.8 dB. Therefore the peak response to the sand alone is less than the sidelobe response to the target.

These preliminary results indicate a favorable chance for success in imaging of subsurface mines with a focused synthetic aperture array. Future experimental plans include the use of targets of varying dielectric constant including real mine casings, experiments in a moist sand medium, further forward and backscattering experiments for additional angles and ranges, and additional array imaging experiments under these conditions. A 1 nsec pulse capability gives improved range resolution. The addition of S-band capability to allow higher resolution imaging is suggested.

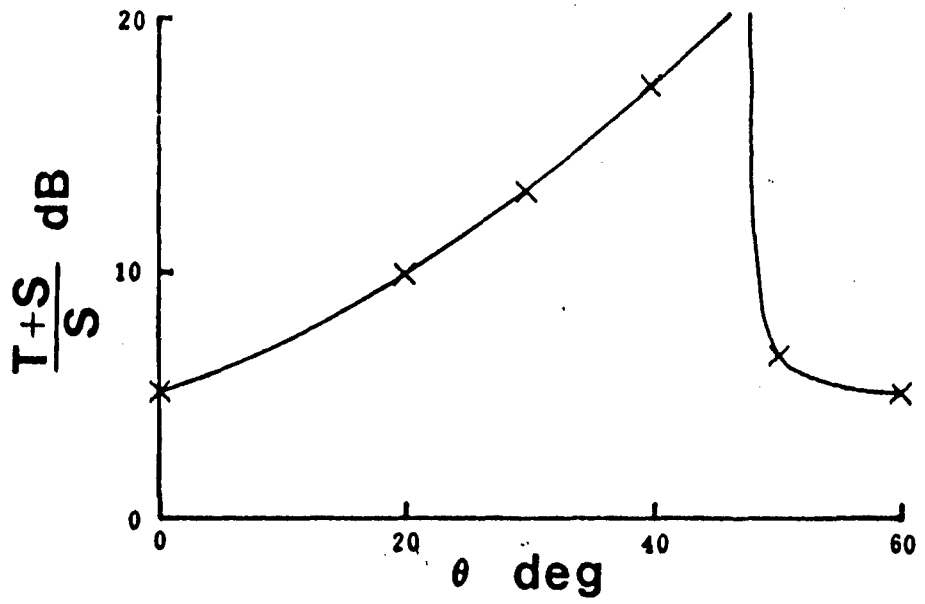

Figure 3.5. Ratio of forward reflection of buried metal target (T) to sand (S) vs. angle of incidence.

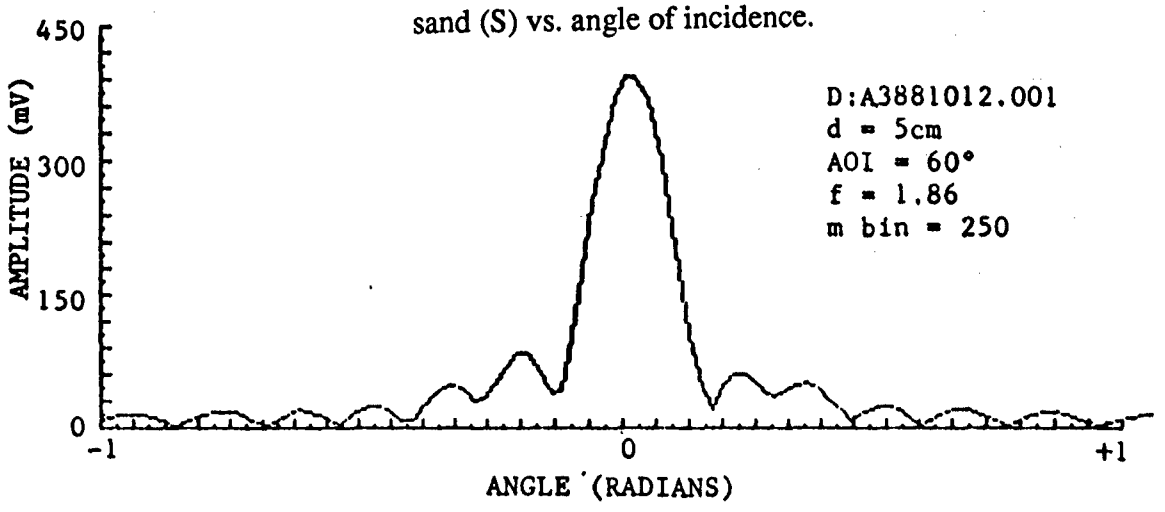

Figure 3.6. Buried Metal Plate.

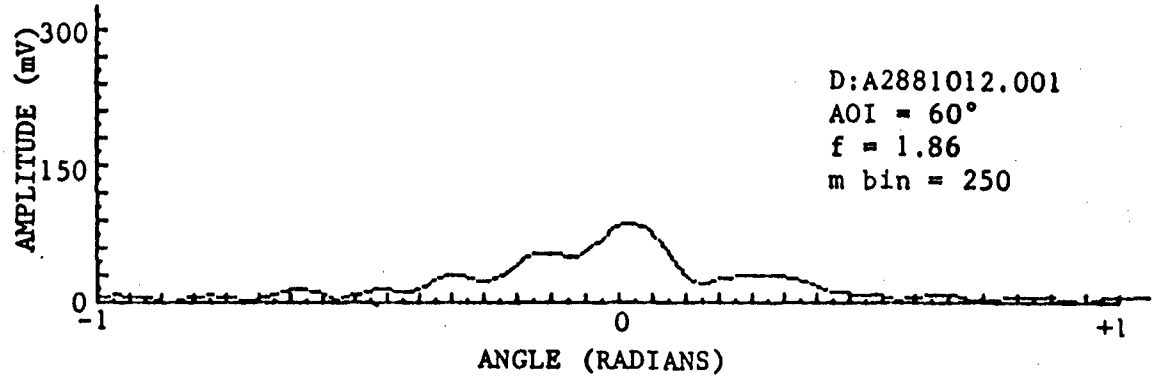

Figure 3.7. Sand Alone.

2.4 L-Band Mine Detection Experiments

The outdoor L-band mine detection measurements continued after the completion of the indoor mine radar cross-section measurements. The objective of the measurements was to verify the Brewster angle effect on reduction of reflected energy in a bistatic oblique forward scattering mode. It had been found during the indoor RCS measurements that the direct path radiation between antennas was large enough to cause error in the measurements. A centrally located absorber was used between the transmit and receive antennas to successfully eliminate the direct path interference. This same approach was used in the outdoor measurements. A microwave absorber barrier was suspended between the two antennas to block the direct path radiation but allow the ground reflected energy to propagate under the barrier.

Reflection coefficient measurements were made on the sand by varying the angle of incidence between 40° and 75°. A distinct Brewster angle effect was seen in all the measurements, and the reflection coefficient showed a noticeable decrease over the range of 45° to 60° angle of incidence. The minimum measured value of the reflection coefficient was 0.068 at about 60° compared to a value of 0.231 at 45°.

Another method was discovered to reduce surface reflections in bistatic forward scattering. Since the ground surface was in proximity to the transmit and receive antennas, the reflected energy distribution was approximately the geometrical projection of the transmit horn aperture. Since the measured scattering from the mines had been found to be wide angle, it was actually possible to place the receive antenna such that it was just outside of the surface-reflected tube of energy from the transmitter but still near the maximum of the mine scattering pattern.

This technique was used to make synthetic aperture measurements of the bistatic forward scattered power from buried mines. The angle of incidence used was 45°. The focal distance of the array was 1.8 m. The results are illustrated in Figures 3.8 - 3.10. Figure 3.8 shows the image as a function of azimuth angle of the surface reflection with no buried mine. The peak level is -14 dB as shown. The square plastic M-19 anti-tank mine was then buried at a depth of 7.5 cm and the image of Figure 3.9 was obtained showing a peak of -9 dB, an increase of 5 dB. This is a large increase in power for this type of mine since its dielectric constant is close to that of sand and it consequently has a low reflectivity. The same procedure was used for the metal anti-tank mine buried at a depth of 5 cm. In this case (see Figure 3.10), the peak power is -2.5 dB, an increase of 11.5 dB over the sand surface reflection alone. These experiments have demonstrated the ability of our technique to detect both types of mine with a high signal-to-clutter ratio.

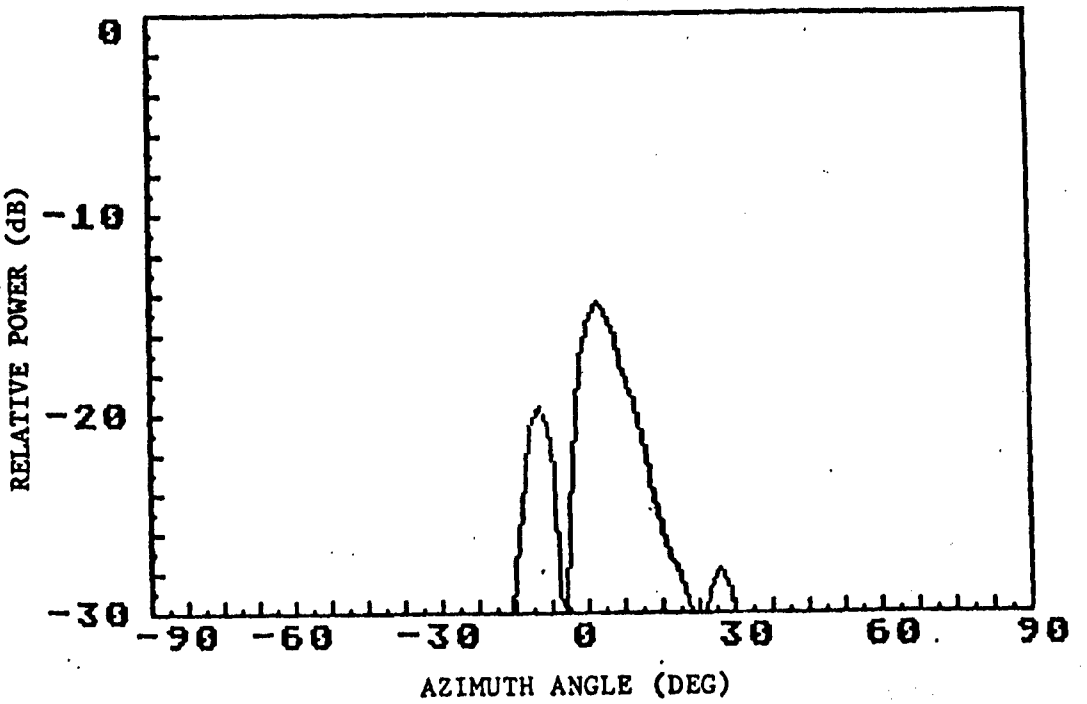

Figure 3.8. SAR Forward Scatter. Sand Alone.
AOI = 45°. Focal Distance = 1.8 m.

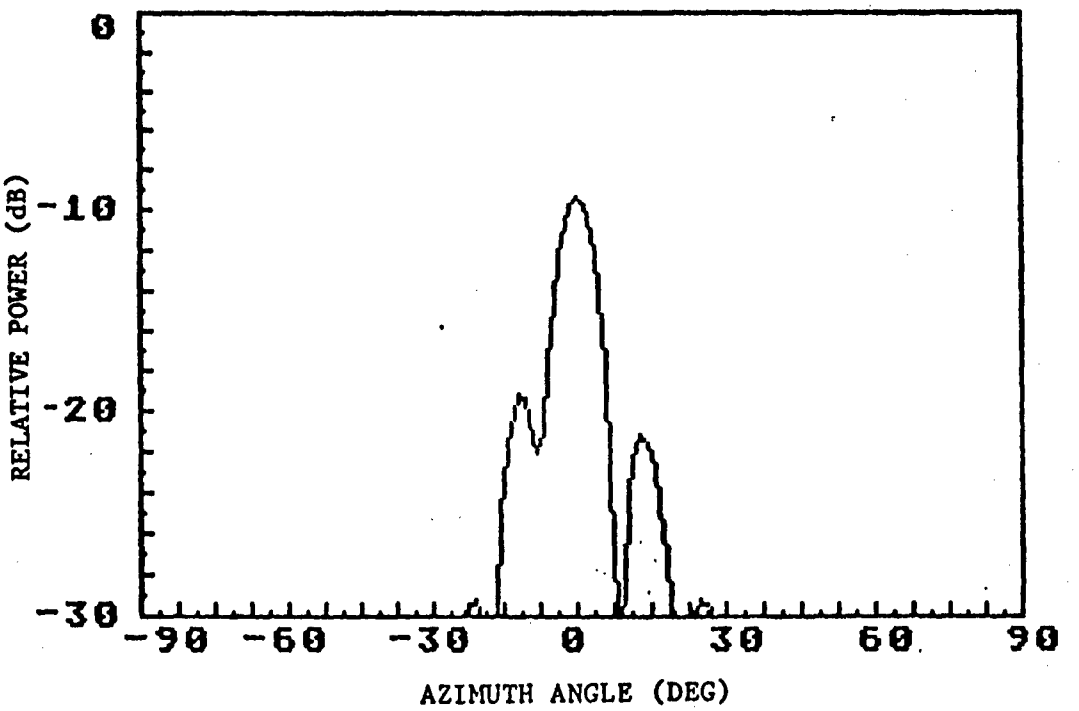

Figure 3.9. SAR Forward Scatter. Plastic Mine.
Depth = 7.5 cm. AOI = 45°. Focal Distance = 1.8 m.

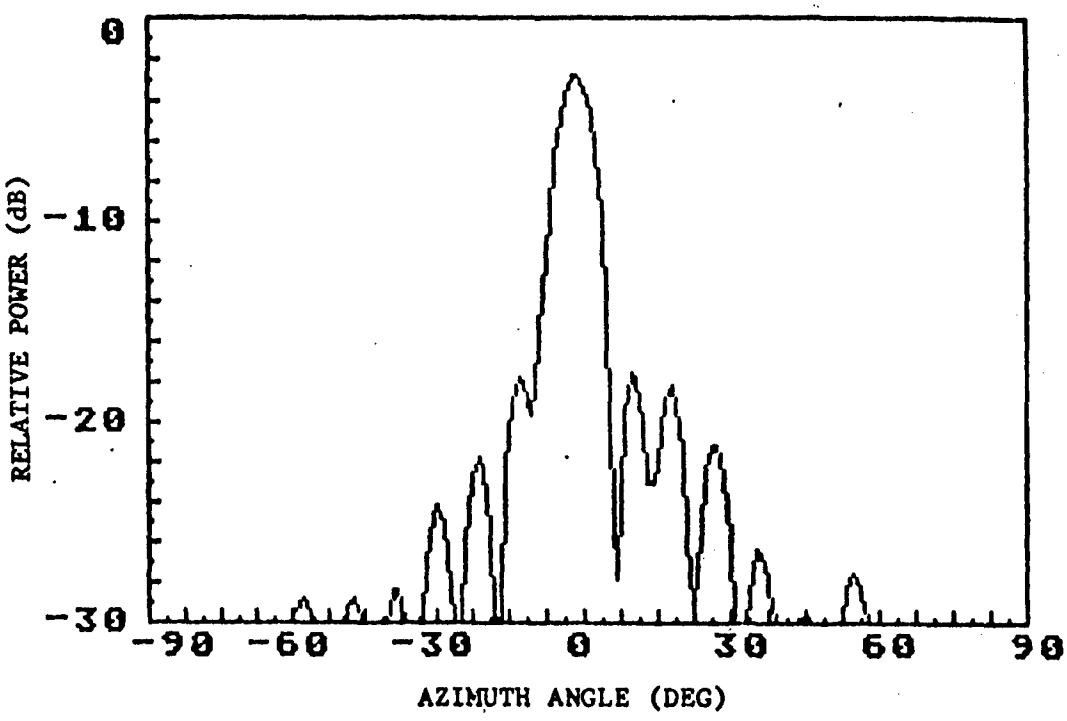

Figure 3.10 SAR Forward Scatter. Metal Mine.
Depth = 5 cm. AOI = 45°. Focal Distance = 1.8 m.

2.5 S-Band Experiments

Experiments were at S-band using a frequency of 3.5 GHz. The experimental hardware is described later in this article. The purpose of increasing the frequency to S-band is to improve the resolution to allow imaging of the mine for identification purposes.

Initial measurements have been made of the forward reflection from the sand surface; these measurements have also shown a significant decrease in reflection at the Brewster angle (55° - 60°). Another valuable feature of the S-band setup is the narrow pulse width of 1 nsec achievable with the diode switch, compared to about 10 nsec at L-band. The greatest advantage of this is the ability to discriminate against the direct path radiation because of its path length difference from the reflected path.

Measurements have also been made of the reflection from buried mines, both with a single receiver, and with the synthetic aperture array. The 1.5 m size of the array aperture is the same as at L-band with the same number of elements, 16, now spaced at about 1 wavelength. Since the field of view of the array is only about 45°, the grating lobe at 90° will not be visible. These data have been analyzed and are discussed in following sections.

2.6 Mine Scattering

The purpose of this task is to determine the forward reflection characteristics of anti-tank mines by analysis of experimental data. Experiments have been performed with metal and plastic mines in both free-space and in soil. A horizontal line array was also used with buried mines to determine their detectability in an oblique forward scattering mode near the Brewster angle. The measurements were made at L-band (1.55 Ghz) and S-band (3.5 Ghz). The soil measurements used sand with varying amounts of moisture.

2.6.1 Radar Cross-Section Measurements

Measurements of the radar cross-section as a function of angle of incidence were performed at L-band for both metal and plastic anti-tank mines. The purpose was to determine if the mines had a significant forward reflected signal when the transmitter was located at an oblique angle of incidence and the receiver was at the opposite angle of reflection with the mine in between, as in the geometry of Figure 3.11. The measurements were made at vertical polarization (electric field in the plane of incidence) which is the system polarization to be used for the Brewster angle effect. Monostatic backscattering measurements were also made for

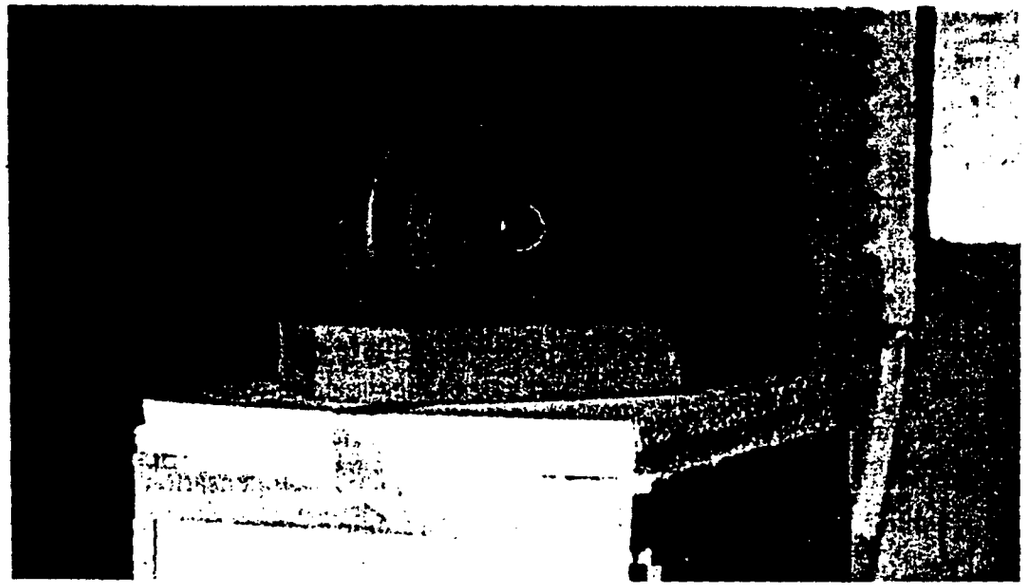

Figure 3.11(a). Support Mounting of Mine, for Experiment.

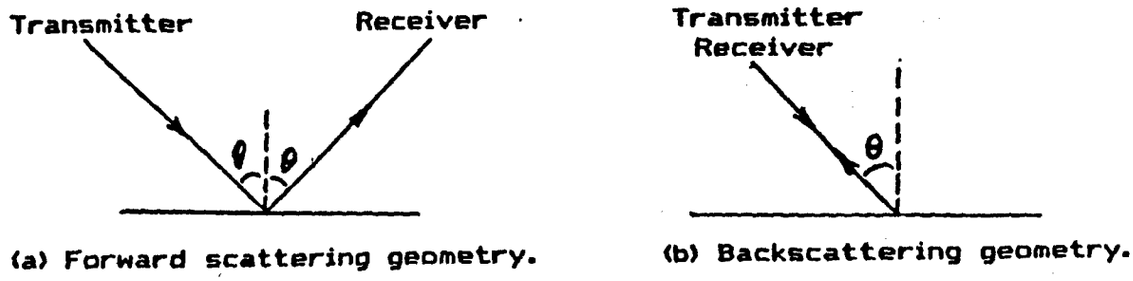

Figure 3.11(b). Scattering Geometry.

comparison. The measurements were made in free space using a narrow pulse so that all other reflections were eliminated.

The results show an almost constant return from the mines as a function of angle of incidence for the forward scattering mode out to wide angles. Since the angle of incidence on the mines would be smaller when they are buried due to refraction, the results show that the oblique forward reflection from a mine would be the same as normal incidence. Typical forward scattering results for the metal M15 mine and the plastic M19 mine are shown in Figures 3.12 and 3.13. Figure 3.12 is the RCS at an L-band frequency of 1550 MHz as a function of angle of incidence on the plane of the mine (same as angle of reflection) and is almost constant at its maximum out to 30°. Since the angle of refraction in soil is less than 30° for angles of incidence of less than 60°, the forward reflection from the mine would be almost constant at all oblique angles of incidence. Figure 3.13 is the corresponding result for the M15 and shown similar behavior.

These are in contrast to backscattering shown in Figures 3.14 and 3.15 in which the transmitter and receiver are at the same location. The reflected backscatter signal decreases rapidly as the angle of incidence on the plane of the mine increases beyond 5°. Similar results were obtained at a frequency of f=1300 MHz with both mines.

The S-band forward scattering results at 3500 MHz are given in Figures 3.16 and 3.17. Figure 3.16 shows the M15 scattering decreasing slightly beyond normal incidence, and then continually increasing to its maximum level at wide angles. The M19 result in Figure 3.17 shows a relatively constant level out to wide angles. The backscattering results of Figures 3.18 and 3.19 demonstrate a series of rapid variations between maxima and minima. The case of the M19 shown a main backscattering lobe only 5° wide.

These results demonstrate the realiability and consistency of high scattering levels at wide angles in a bistatic forward scattering mode. Measurements at horizontal polarization showed similarly high wide angle scattering.

2.6.2 Buried Mine Measurements

The mine forward scattering measurements were also performed in dry and moist sand for fixed angle of incidence and varying mine depth. A summary of some of the results is given in Table 1. The ratio of the signal-to-clutter of the mine reflection to the soil reflection is given as S/C. The M15 metal mine has an expected high forward scattering level at both frequencies. The plastic M19 has a lower return but would still be detectable, especially when an array is used.

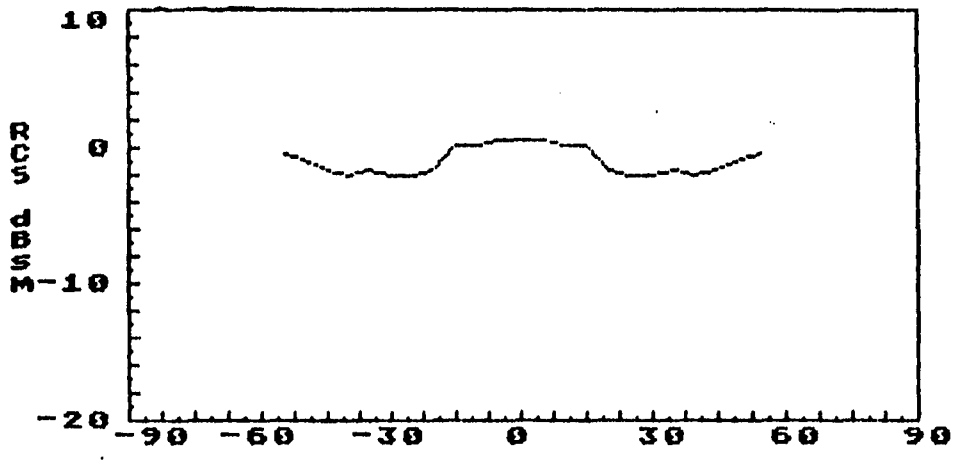

Figure 3.12. Forward Scattering RCS of Metal Mine at L-Band.

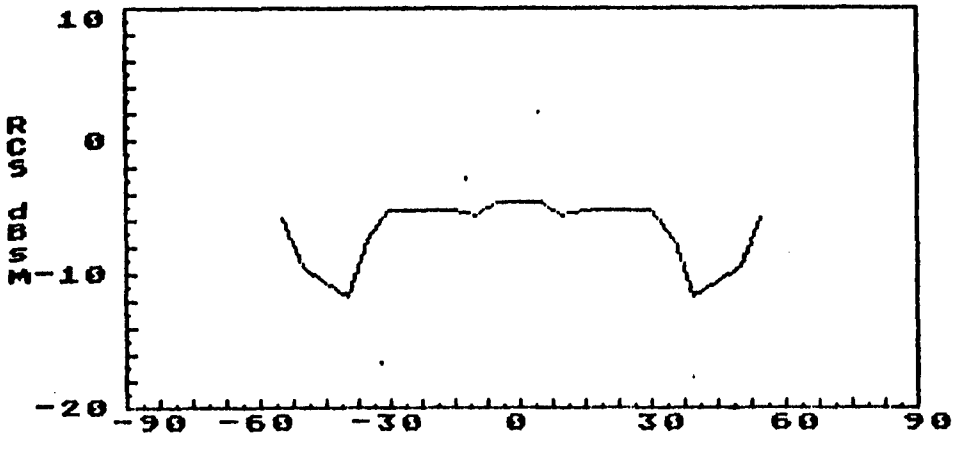

Figure 3.13. Forward Scattering RCS of Plastic Mine at L-Band.

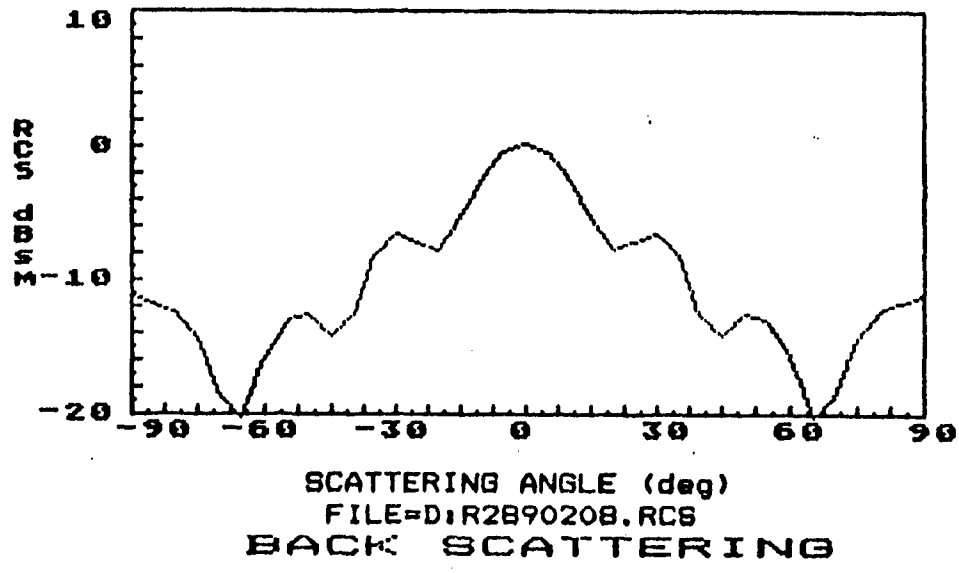

Figure 3.14. Backscattering RCS of Metal Mine at L-Band.

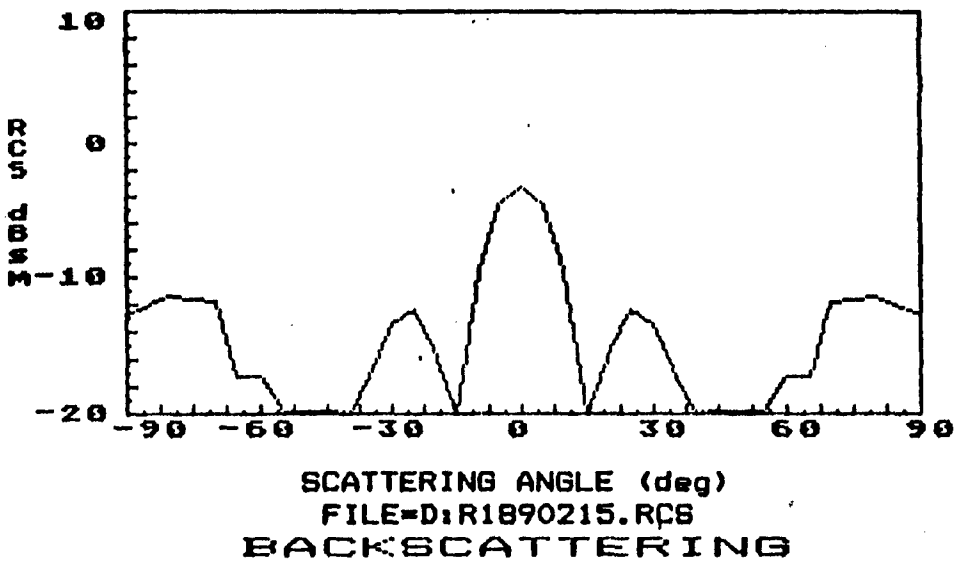

Figure 3.15. Backscattering RCS of Plastic Mine at L-Band.

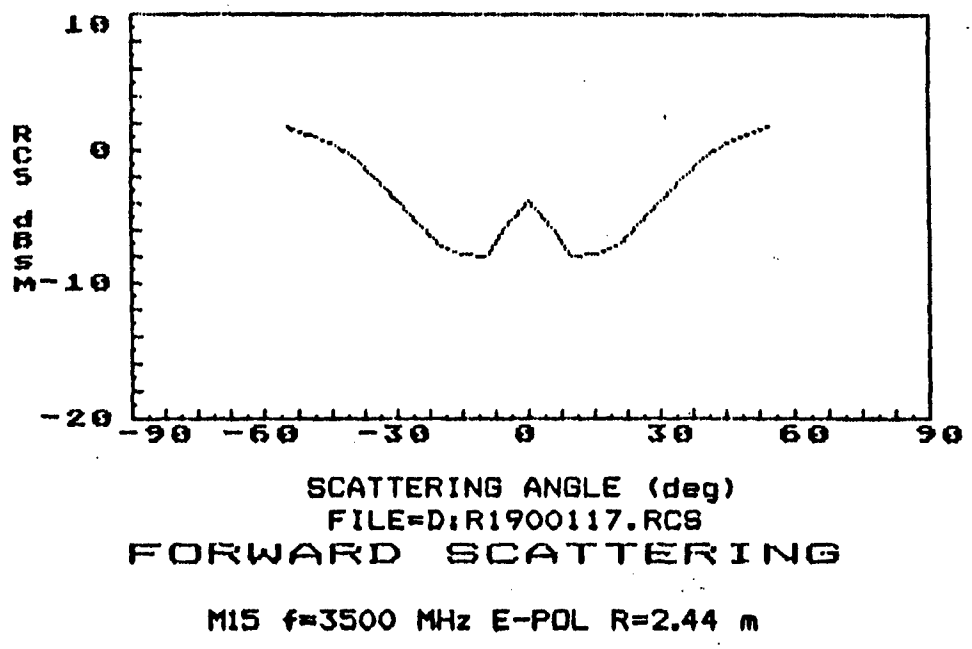

Figure 3.16. Forward Scattering RCS of Metal Mine at S-Band.

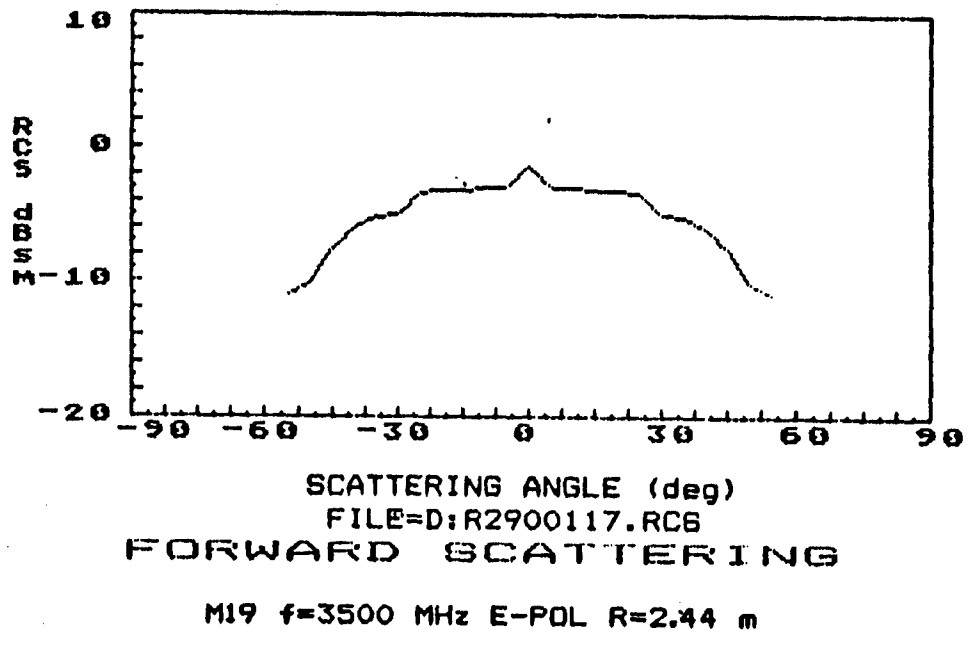

Figure 3.17. Forward Scattering RCS of Plastic Mine at S-Band

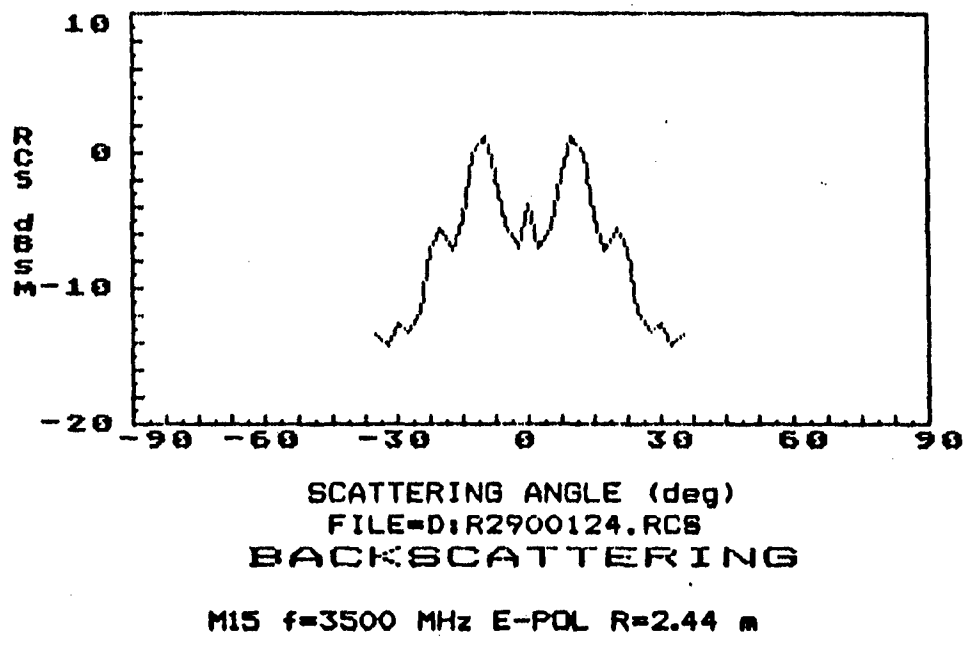

Figure 3.18. Backscattering RCS of Metal Mine at S-Band.

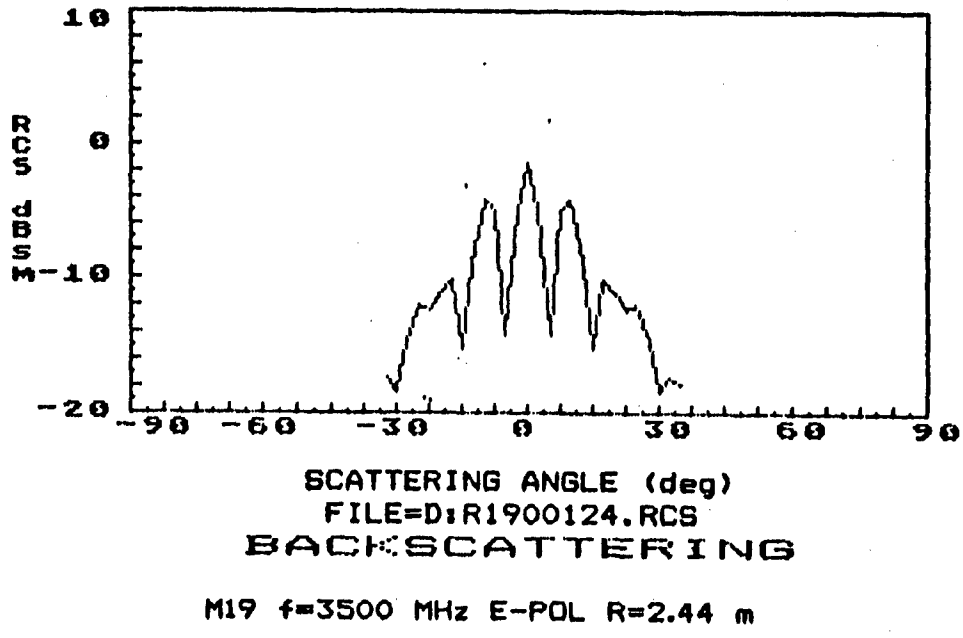

Figure 3.19. Backscattering RCS of Plastic Mine at S-Band.

Table 1. Peak Reflection Levels

L-Band (1.55 GHz) 0% water

Mine	R	AOI		d	S/C
M15	1.8m	45°	5 cm	12 dB	
M19	1.8m	45°	7.5 cm	5 dB	

S-Band (3.5 GHz) 0% water

Mine	R	AOI		d	S/C
M15	1.2m	55°	3.8 cm	20 dB	
M19	1.2m	55°	3.5 cm	5 dB	

S-Band (3.5 GHz) 10% water

Mine	R	AOI		d	S/C
M19	1.2m	55°	3.8 cm	4 dB	

2.6.3 Focused Array Measurements

Focused array measurements were performed using the forward scattering horizontal line array setup. The arrays were synthesized by sequentially moving a single antenna to each of the desired array element locations and sampling the element I and Q outputs. The array was then digitally focused and scanned to form the images. Experiments were performed using a 16 element L-band array and a 22 element S-band array. The array response results show detectibility of both metal and plastic buried mines at L-band but no shape information due to the long wavelength (20 cm). In contrast, the S-band array data shown a distince variation in level while scanning over the surfaces of both metal M15 and plastic M19 buried mines. This is an initial demonstration of the ability to obtain shape information for buried mines at S-band frequencies.

These S-band measurements of anti-tank mines buried in sand were made using a bistatic S-band radar system having a wide beam standard gain horn as the illuminating antenna and a 22 element horizontal line array as the receiving antenna. The system used the oblique

forward scattering geometry with the transmit and receive antennas at the 55° Brewster angles of incidence and reflection, respectively. The antennas were at a height above the sand surface of .7 m with a separation of 2.0 m. The targets were individually located centrally between the transmit and receive antennas, and the baseband I and Q element data was sampled by the 20 GHz HP54120T sampling oscilloscope. Focused array digital beamforming was then performed in the cross-range dimension with focusing depth as a parameter. The array was scanned to 100 points in cross-range (transverse horizontal) over a 1 m distance, at each of 25 focal depths in 4 cm increments varying from .2 m above the surface of the ground to .8 m below the surface. The resulting data was then converted to power, quantized into 16 levels, and a half-tone gray-level image was generated for each target with power decreasing from white to black.

The image in Figure 3.20 shows the response of the array to the sand in the absence of any target, where the image is normalized to its own peak (voltage) amplitude of 23 (in relative units). The image in Figure 3.21 is that of a 1 in wide metal ruler oriented longitudinally on the surface of the sand in order to test the resolution capability of the array. The data is normalized to its peak amplitude value of 133, thus the sand surface reflection is below the lowest quantization level and is invisible. From the actual amplitude data the resolution is ascertained to be 7.5 cm. The theoretical depth of field, (depth resolution) appears to be near its theoretical value of 30 cm. The peak intensity of the image also appears correctly at the location of the surface. The image of Figure 3.22 is that of an M15 metal mine buried at a depth of 7.5 cm and again normalized to its peak of 139, with the surface reflection also below the lowest quantization level and appearing black. In this image, there is notable detail across the mine horizontal dimension with the largest reflection for the raised central pressure plate and two secondary reflection lobes from the annulus surrounding the pressure plate. The highest image intensity also occurs at the correct depth of 7.5 cm and occurs significantly lower in position than the peak of the ruler image. Some smearing of the image occurs above the surface since the depth of field is large enough to capture some of the very high reflections from the mine surface even while it is focused above the ground. This phenomenon will not occur with weaker targets, such as the M19 plastic mine also at a depth of 7.5 cm, shown in Figure 3.23. The peak relative amplitude of the mine is 47, and normalization t this peak now shows some of the sand reflections appearing as clutter on the image. In order to improve the image before a interpretation, the sand reflection was removed. The interfering sand reflection is illustrated in Figure 3.24 which is the same data as the image in Figure 3.20 but now normalized to the peak of the M19. Thus it is the actual surface clutter appearing in the M19 image. If the threshold is now raised by three quantization levels so the lowest level

is now above the peak surface reflection, an improved image of the M19 now results as shown in Figure 3.25. Now the detail is apparent across the mine surface with the peak lobe again appearing at the top pressure plate (probably due to the air gap), with slightly lower lobes at the top sides of the mine. The peak again occurs at the actual mine depth.

The above images demonstrate that both metal and plastic buried mines can be detected and shape information can be obtained using a high resolution array at S-band with bistatic oblique forward scattring near the Brewster angle. The images also indicate that the signatures of the two mines are different and also characteristic, suggesting the ability to identify mine type by the image signature.

2.6.4 Conclusions

The results of this task are very important since they demonstrate the feasibility of detecting, imaging and identifying buried metal and plastic mines using a focused array in a bistatic forward scattering geometry. Further improvement in the images could be obtained with more sophisticated image processing techniques.

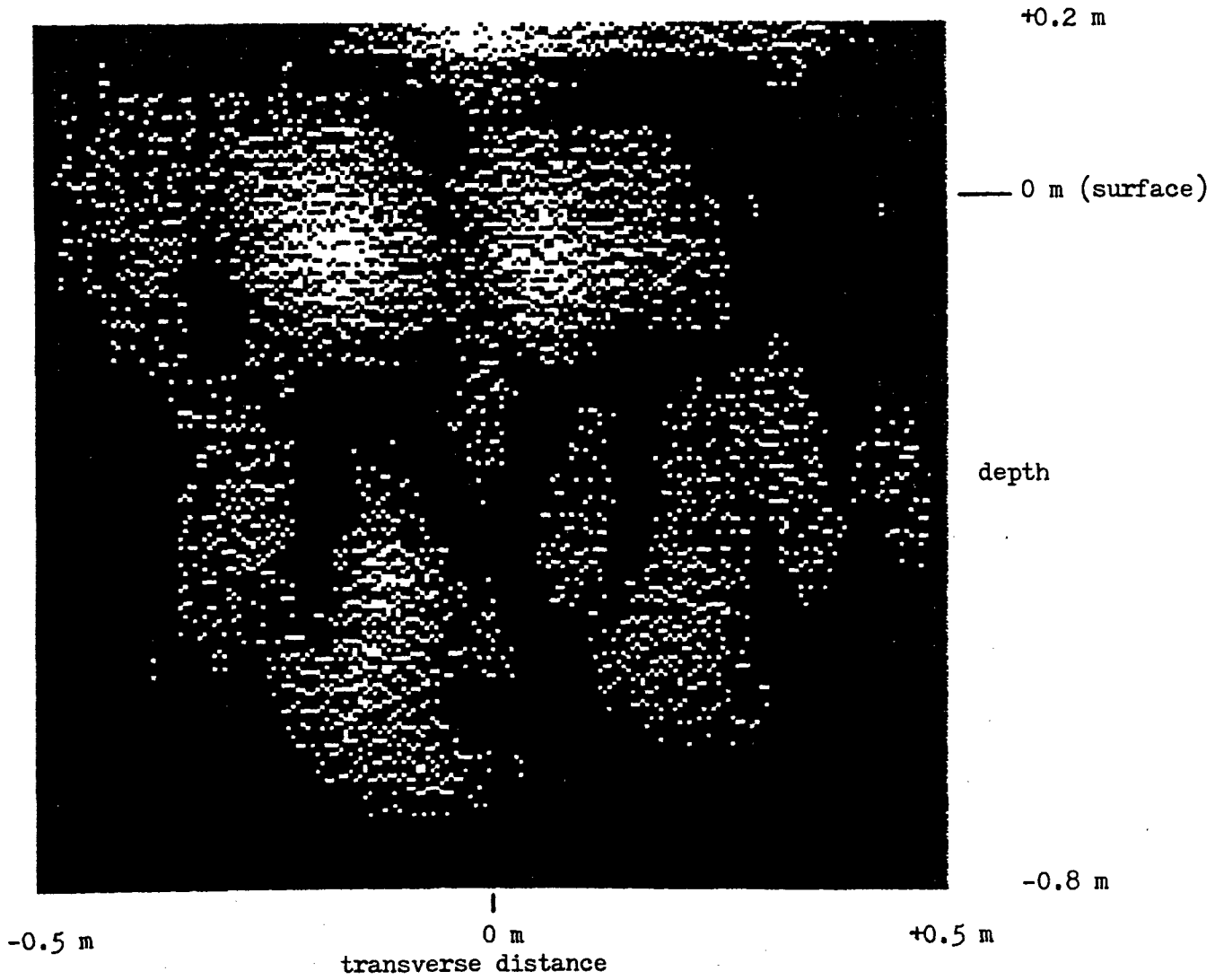

Figure 3.20. Focused line array image of soil reflections.

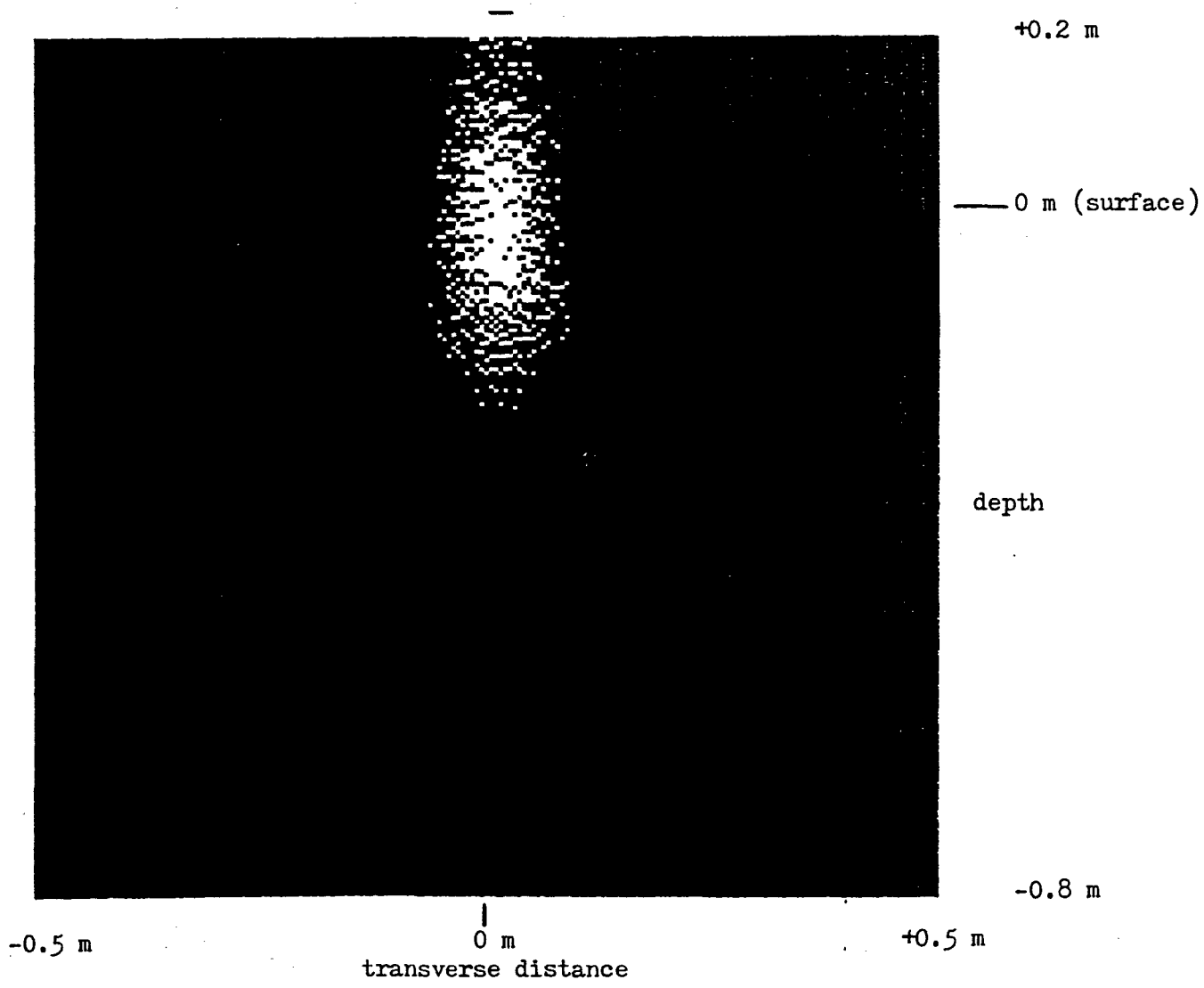

Figure 3.21. Focused line array image of ruler on surface.

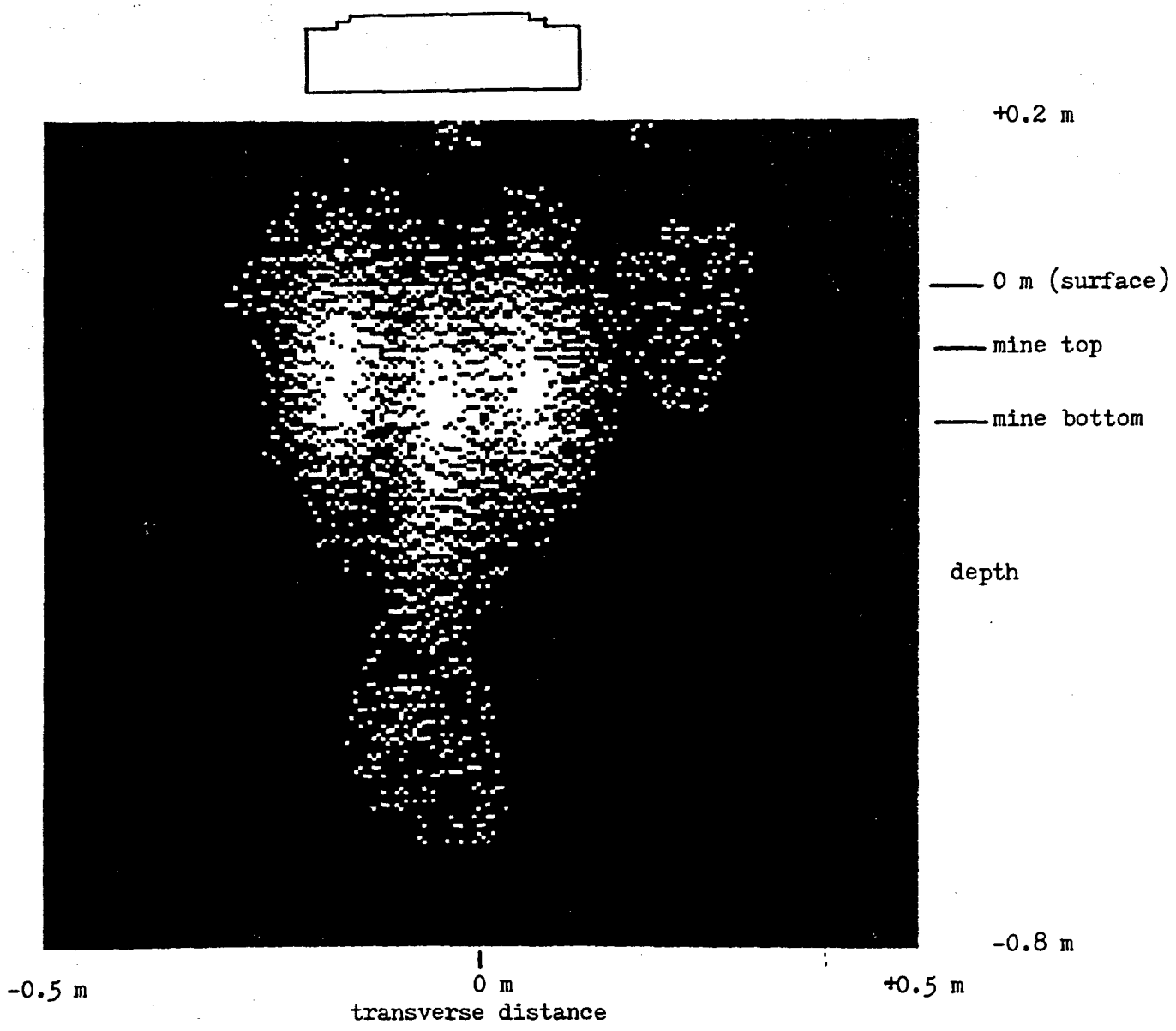

Figure 3.22. Focused line array image of M15 at 7.5 cm depth.

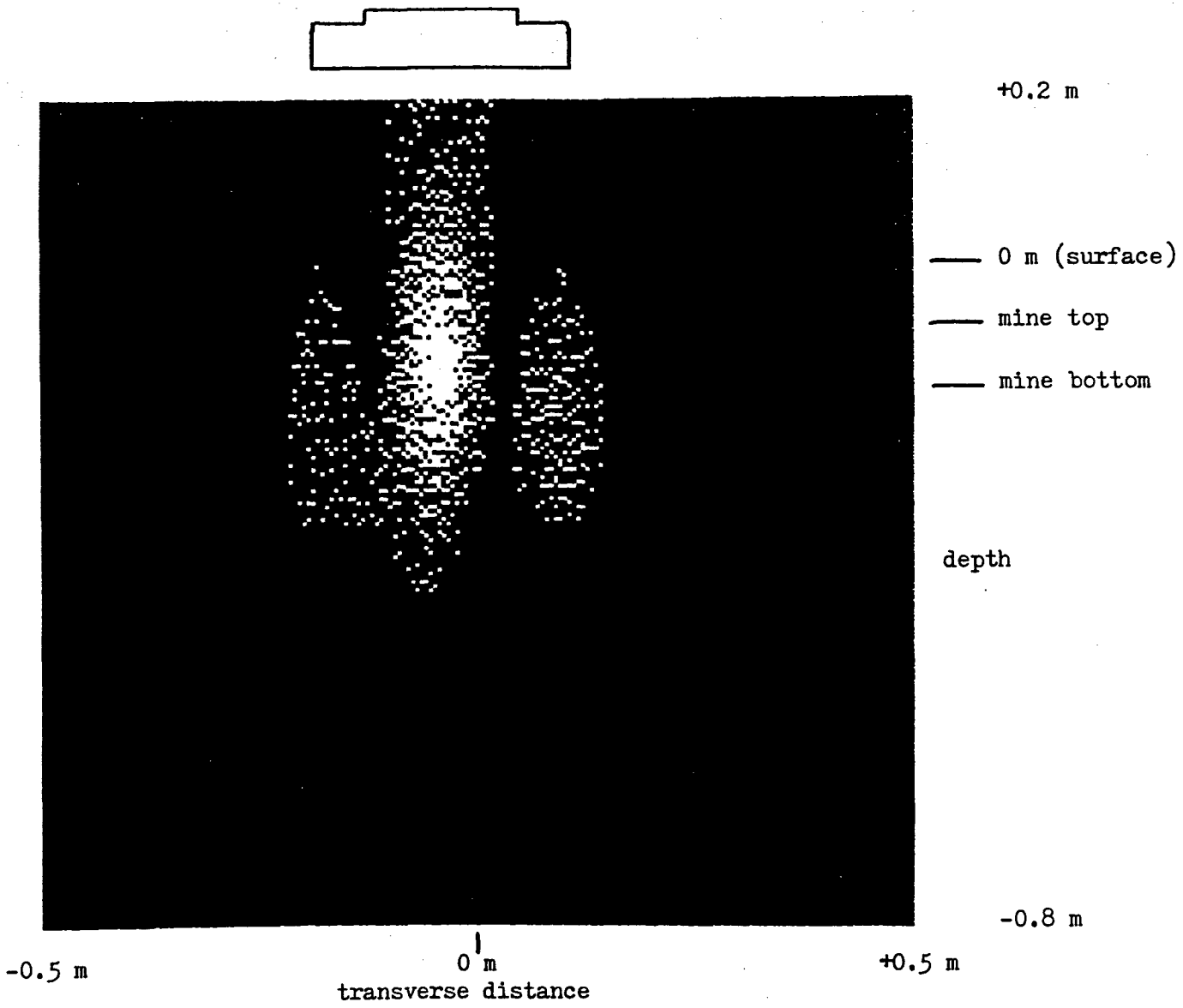

Figure 3.23. Focused line array image of M19 at 7.5 cm depth.

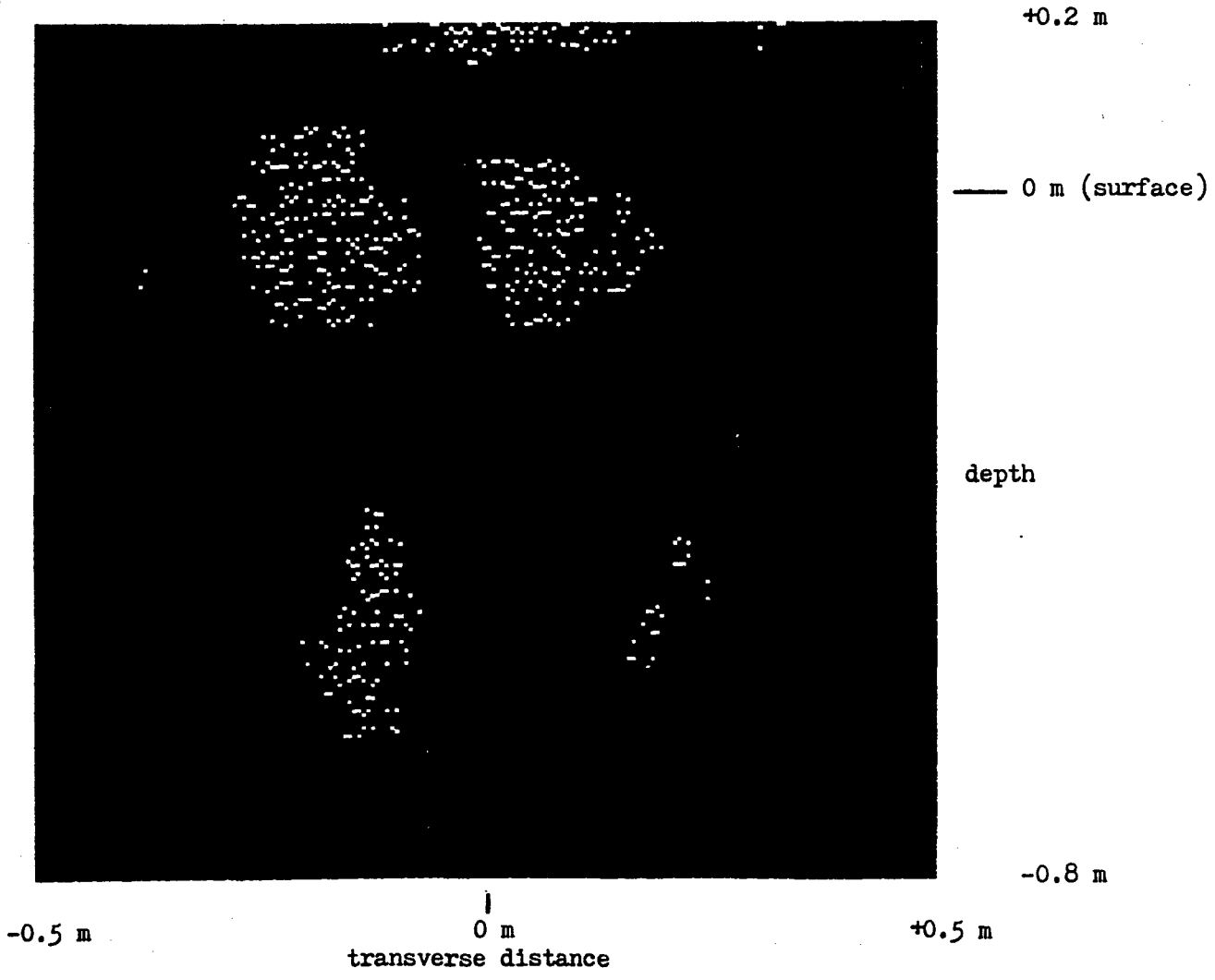

Figure 3.24. Focused line array image of soil reflections normalized to M19.

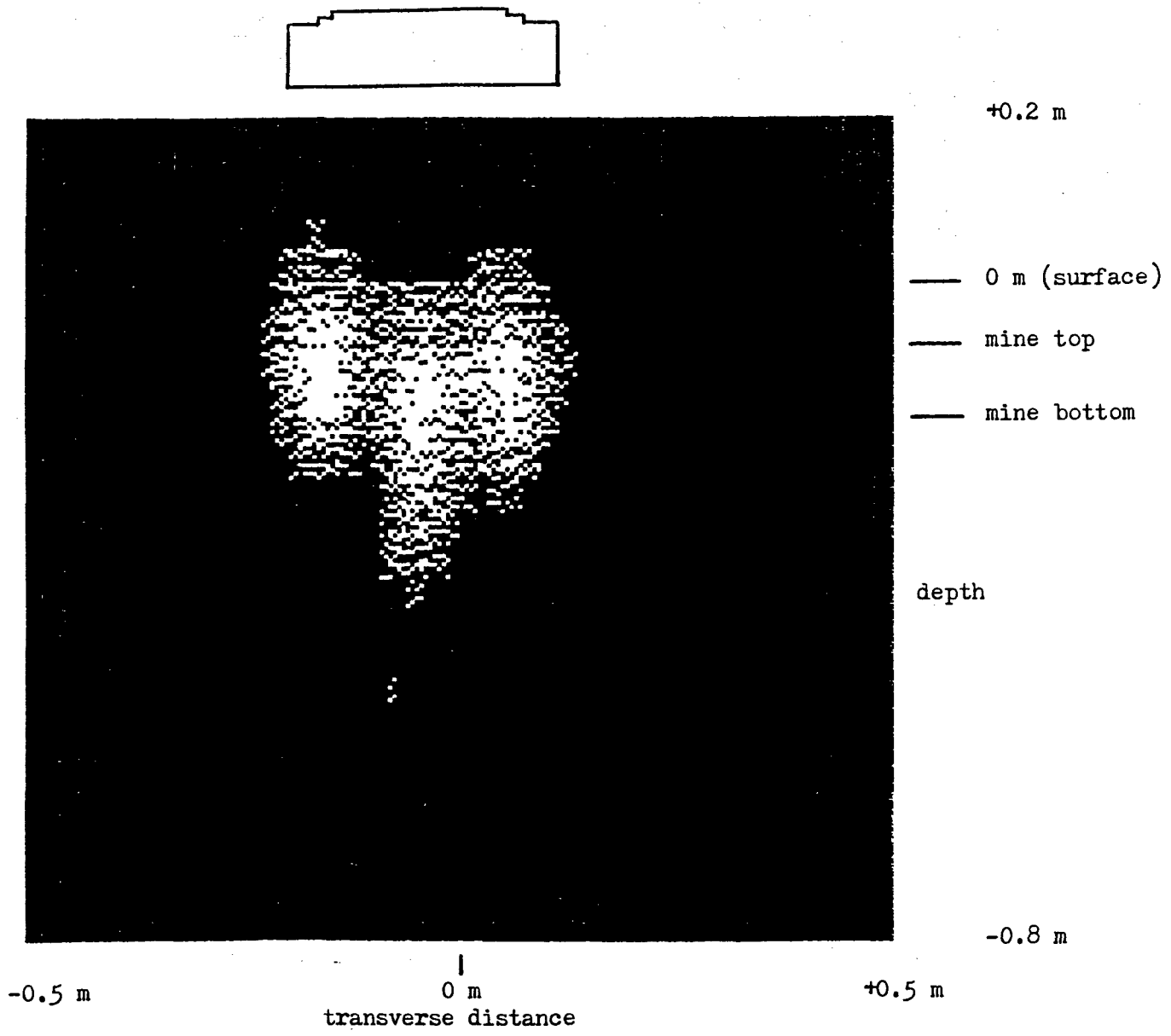

Figure 3.25. Focused line array image of M19 with soil reflections removed.

2.7 Propagation Model

2.7.1 Objective

The pupose of this task is to devleop a propagation model for oblique forward scattering from soil and to compare measured data with the model. The objective is to determine the effectiveness of the Brewster angle effect in reducing or eliminating soil surface reflections.

2.7.2 Propagation Model

A theoretical propagation model based on Stratton [9] has been developed which predicts soil transmission and reflection parameters including amplitude, phase and index of refraction variations. The model can be used for arbitrary polarization, angle of incidence and soil conductivity and dielectric constant. A computer model has been implemented to readily compare the theory with experimental measurements.

Measurements using dry and moist sand have been performed to verity the Brewster angle effect. The same forward scattering geometry is used as for the previous experiments, i.e., with the transmit antenna directed forward to the soil suface at the angle of incidence, with the receiver symmetrically located at the angle of reflection on the other side of the incident point. The angle of incidence was then varied for the measurements by moving the transmitter antenna position to the angle of reflection. The measurements were performed with polarization in the plane of incidence (vertical) since a vertically polarized wave at the Brewster angle would be completely transmitted into the soil.

Figures 3.26 - 3.29 compare the results of the theoretical model with the measured data. They show the reflection coefficient of the electric field as a function of the angle of incedence. Figure 3.26 is the theoretical result for L-band with sand containing 5% water. The reflection coefficient becomes very small between 60° and 65°. The corresponding measured data is shown in Figure 3.27 and agrees with the general characteristics of the model. Figure 3.28 shows the theoretical S-band result for dry sand having zero reflection coefficient at the Brewster angle which occurs at 58°. The measured data of Figure 3.29 shows good agreement and has a minimum reflection coefficient of about .03 at 55°.

2.7.3 Conclusion

This task has demonstrated conclusively a substantial reduction of soil surface reflections for a foward scattering system using vertical polarization at the Brewster angle. The results are valid for both dry and moist soil, the moist soil having a minimum reflection coefficient slightly above zero at an angle somewhat larger than the Brewster angle.

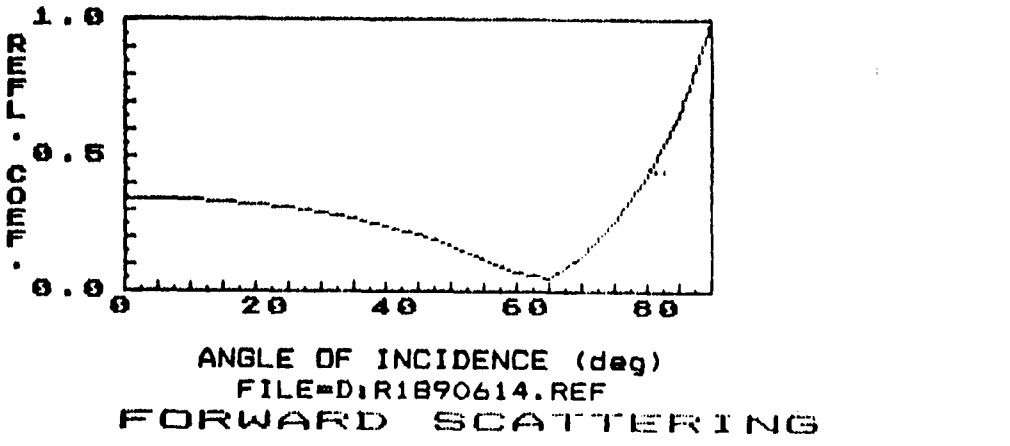

Figure 3.26. Theoretical soil reflection coefficient at L-band.

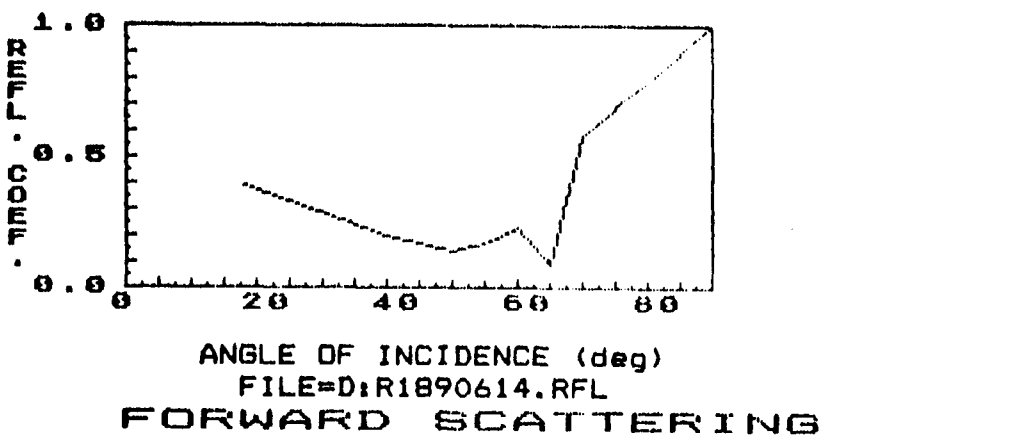

Figure 3.27. Measured soil reflection coefficient at L-band.

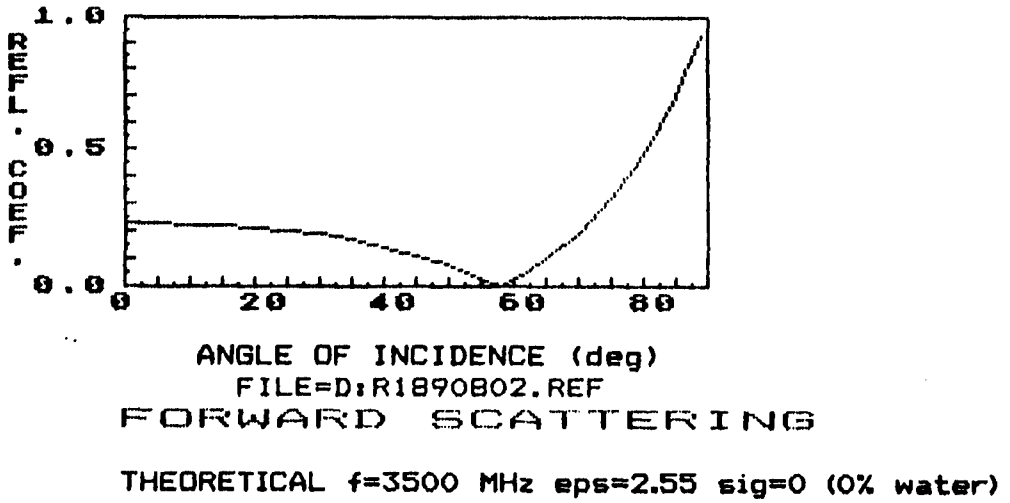

Figure 3.28. Theoretical soil reflection coefficient at S-band.

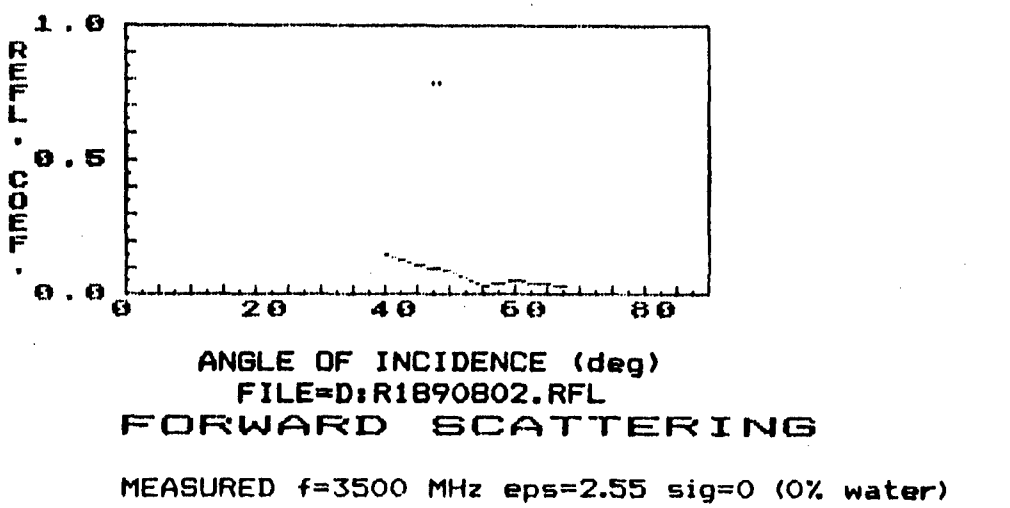

Figure 3.29. Measured soil reflection coefficient at S-band.

3. Bibliography

[1] R. S. Berkowitz et. al. "Report on the Experimental Program: Subsurface Radar for Mine Detection," VFRC Quarterly Progress Rpt. No. 55, April-June 1988, pp. 58-64.

[2] R. S. Berkowitz et. al. "Applictions of Subsurface Radar for Mine Detection," VFRC Quarterly Progress Rpt. No. 56, July-Dec. 1988, pp. 5-13.

[3] R. S. Berkowitz et. al. "Applictions of Subsurface Radar for Mine Detection," VFRC Quarterly Progress Rpt. No. 57, Jan.-Mar. 1989, pp. 6-23.

[4] R. S. Berkowitz et. al. "S-band equipment for Subsurface Radar for Mine Detection," VFRC Quarterly Progress Rpt. No. 58, April-Sept. 1989, pp. 7-9.

[5] R. S. Berkowitz et. al. "Applictions of Subsurface Radar for Mine Detection," VFRC Quarterly Progress Rpt. No. 59, April-Sept. 1989, pp. 10-13.

[6] S. Roy et al. "Subsurface Radar for Buried Target Detection," IEEE International Radar Conference, Arlingtion, VA, 1990, pp. 129-134.

[7] C. A. Balanis, "Advanced Engineering Electromagnetics," John Wiley, New York, 1989.

[8] R. M. Lerner, "The Theoretical Basis of Geodar," MIT Lincoln Lab Rpt., Aug. 1967.

[9] J. A. Stratton, "Electromagnetic Theory," McGraw-Hill, New York, 1941.

[10] J. E. Hipp, "Soil Electromagnetic Parameters as Functions of Frequency, Soil Density and Soil Moisture," Proc. IEEE, vol. 62, no. 1, Jan. 1974, pp. 98-103.

[11] L. C. Chan, D. L. Moffatt and L. Peters, "A Characterization of Subsurface Radar Targets," Proc. IEEE, vol. 67, no.7, July 1979.

[12] P. Beckmann and A. Spizzichino, "The Scattering of Electromagnetic Waves from Rough Surfaces," Artech House, Mass. 1987.

[13] G. Tricoles, R. A. Hayward et al., "Nearfield Electromagnetic Detection of Mines," Rpt. No. R-87-013, General Dynamics, Dec. 1987.

[14] L. Tsang, J. A. Kong and R. T. Shin, "Theory of Microwave Remote Sensing," John Wiley, 1985.

[15] D. A. Hill, "Near Field Detection of Buried Dielectric Objects," IEEE Trans. Geosc. & Rem. Sensing, vol. 27, July 1989, pp. 364-368.

List of Personnel & Publications

R. S. Berkowitz	Co-Principal Investigator
S. Roy	Co-Principal Investigator
W. J. Graham	Subcontractor
D. Carlson	Research Specialist
W. Borders	Technician
T. S. Kim	Graduate Student
T. Ozdemir	Graduate Student

[1] R. S. Berkowitz et. al. "Report on the Experimental Program: Subsurface Radar for Mine Detection," VFRC Quarterly Progress Rpt. No. 55, April-June 1988, pp. 58-64.

[2] R. S. Berkowitz et. al. "Applictions of Subsurface Radar for Mine Detection," VFRC Quarterly Progress Rpt. No. 56, July-Dec. 1988, pp. 5-13.

[3] R. S. Berkowitz et. al. "Applictions of Subsurface Radar for Mine Detection," VFRC Quarterly Progress Rpt. No. 57, Jan.-Mar. 1989, pp. 6-23.

[4] R. S. Berkowitz et. al. "S-band equipment for Subsurface Radar for Mine Detection," VFRC Quarterly Progress Rpt. No. 58, April-Sept. 1989, pp. 7-9.

[5] R. S. Berkowitz et. al. "Applictions of Subsurface Radar for Mine Detection," VFRC Quarterly Progress Rpt. No. 59, April-Sept. 1989, pp. 10-13.

[6] S. Roy et al. "Subsurface Radar for Buried Target Detection," IEEE International Radar Conference, Arlingtion, VA, 1990, pp. 129-134.

[7] T. Ozdemir et al. "Exact Solutions for the Propagation Time in Bistatic Radar Geometry for Subsurface Imaging Applications,"Digest of The IEEE Eighth Annual Benjamin Franklin Symp., Philadelphia, PA, 1990, pp. 44-47.

[8] T. Ozdemir et al, "A Bistatic System for Imaging of Shallow Subsurface Objects," submitted to IEEE Trans. Geosci. Remote Sensing.

COMPUTER PROGRAMS USED IN THE MINE DETECTION PROJECT*

September, 1990

Tayfun Özdemir
Valley Forge Research Center
Moore School of Electrical Engineering
University of Pennsylvania
Philadelphia, Pennsylvania 19104

* This work was supported by the Army Research Office, Research Triangle Park, NC 27709-2211, under Contract No. DAAL03-87-K-10119, with the cooperation of the Army Research Laboratory, Ft. Belvoir, VA 22060-5606.

COMMON TO ALL PROGRAMS

(a) Programing Language

Programs have been written in FORTRAN 77 programing language.

(b) Location

The programs are stored in the account named *ozdemir* on the Electrical Engineering Department branch of the main frame computer named *pender* located at the School of Engineering and Applied Science of the University of Pennsylvania. They are also available on 5" and 3.5" floppy disks provided.

(c) Execution

(i) To execute the program *image.f*, for example, on the main frame computer *pender*, first, to compile it, type "f77 image.f". If no errors are detected, then type "a.out" to run it.

(ii) To execute a program on an IBM PC, first move the program file and all the input files to the directory that has the fortran compiler applications. The file containing the program must have the extention "*.for*". So, to execute the program *image.for*, for example, type "for1", press RETURN, type "image", and press RETURN four times. If no errors are detected, type "pas2", press RETURN. If no errors are detected, type "link", press RETURN, type "image", and press RETURN four times. If no errors are detected, just type "image" and press RETURN to run the program.

(d) Coordinate Sign Convention

The coordinate sign convention is given in Figure 1 and used by the programs described here for identifying the air and the subsurface media.

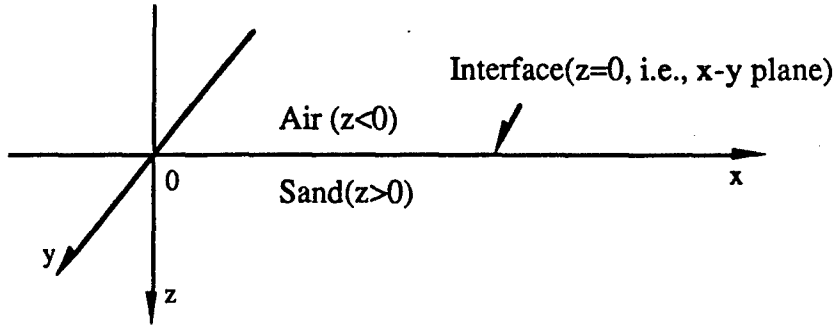

Figure 1: Coordinate Sign Convension

(e) Flexibility

The programs provide quite a deal of flexibility for imaging setup in the sense that transmitter, scan points and receiver elements can be in either medium (air or subsurface medium.) Only serious constraints upon the imaging setup are that the transmitter is a single point element, and that the receive array is linear, periodic and parallel to one of x, y or z axes.

The way they are presented here, the programs are consistent with each other in terms of formating for the flow of data between the programs. The samples of input and output files are available in the respective directories. The *sample* data in the input files are in accordance with the current imaging setup and the system parameters.

(f) Units

MKS unit system is used. Any exceptions are cited wherever appear.

PROGRAM #1: *interface.f*

Location: *ozdemir/research/interface*

1.1 CODE

```
c     THIS SUBROUTINE CALCULATES THE LENGTHS OF THE AIR AND THE SUBSURFACE
c     PARTS OF THE RAY PATH BETWEEN TWO SEPERATE POINTS (P1 AND P2) IN A MEDIA
c     COMPOSED OF AIR AND A SUBSURFACE MEDIUM, EACH OF WHICH IS A HOMOGENOUS,
c     ISOTROPIC, NONMAGNETIZABLE AND CONDUCTING (EXCEPT FOR AIR, WHICH IS
c     NONCONDUCTING) MEDIUM, SEPERATED BY A PLANAR INTERFACE. THE POINTS CAN BE
c     IN DIFFERENT MEDIUMS AS WELL AS IN THE SAME MEDIUM. THE INTERFACE IS THE
c     Z=0 OR (X-Y) PLANE. POINTS WITH Z<=0 ARE IN THE AIR MEDIUM WHILE POINTS
c     WITH Z>0 ARE IN THE SUBSURFACE MEDIUM.
c
c
c     THE PARAMETERS AND THE VARIABLES USED IN THE PROGRAM:
c
c     eps (INPUT PARAMETER) : RELATIVE DIELECTRIC CONSTANT OF THE SUBSURFACE
c                             MEDIUM (>=1)
c     sig (      "        ) : CONDUCTIVITY OF THE SUBSURFACE MEDIUM [mho/meter]
c     f   (      "        ) : FREQUENCY OF RADIATION [GHz]
c     x1  (      "        ) : X-COORDINATE OF THE FIRST POINT (P1) [cm]
c     y1  (      "        ) : Y                    "
c     z1  (      "        ) : Z                    "
c     x2  (      "        ) : X-COORDINATE OF THE SECOND POINT (P2) [cm]
c     y2  (      "        ) : Y                    "
c     z2  (      "        ) : Z                    "
c     nit (      "        ) : NUMBER OF ITERATIONS IN CALCULATING THE INCIDENCE
c                             ANGLE
c     eta (OUTPUT PARAMETER): REFRACTIVE INDEX OF THE SUBSURFACE MEDIUM
c                             EVALUATED AT THE CALCULATED INCIDENCE ANGLE
c     d1  (      "        ): THE LENGTH OF THE AIR PART OF THE RAY PATH [cm]
c     d2  (      "        ): THE LENGTH OF THE SUBSURFACE PART OF THE RAY PATH
c                             [cm]
c     theta (INTERMEDIATE VARIABLE) : INCIDENCE ANGLE [rad]
c     phi   (          "          ) : REFRACTION ANGLE [rad]
c     d     (INTERMEDIATE PARAMETER): HORIZONTAL DISTANCE BETWEEN THE POINTS P1
c                                     AND P2 [cm]
c     h     (          "          ): HIGHT OF THE POINT (P1 OR P2) IN THE AIR
c                                     FROM THE INTERFACE [cm]
c     z     (          "          ): DEPTH OF THE POINT IN THE SUBSURFACE
c                                     MEDIUM FROM THE SURFACE (INTERFACE) [cm]
c
c
      subroutine interface(eps,sig,f,x1,y1,z1,x2,y2,z2,nit,eta,d1,d2)
      real eps,sig,f,x1,y1,z1,x2,y2,z2,eta,d1,d2
      integer nit
c
c     REDUCTION OF THE 3-D PROBLEM TO A PLANAR GEOMETRY PROBLEM
c
      d=sqrt((x1-x2)**2.+(y1-y2)**2.)
c
c     IF BOTH POINTS (P1 AND P2) ARE IN THE AIR MEDIUM OR eps=1
c
      if((z1.le.0..and.z2.le.0.).or.eps.eq.1.) then
      d1=sqrt(d**2.+(z1-z2)**2.)
      d2=0.
```

```
      eta=1.
      goto 3
      end if
c
c     IF BOTH POINTS (P1 AND P2) ARE IN THE SUBSURFACE MEDIUM...
c
      if(z1.ge.0..and.z2.ge.0.) then
      d1=0.
      d2=sqrt(d**2.+(z1-z2)**2.)
      eta=1./sqrt(2.)*sqrt(eps+sqrt(eps**2.+(18.*sig/f)*2.))
      goto 3
      end if
c
c     IF THE POINTS ARE IN DIFFERENT MEDIA
c
      if(z1.le.0..and.z2.gt.0.) then
      h=-z1
      z=z2
      goto 1
      else
      h=-z2
      z=z1
      end if
c
c     ITERATION FOR THE INCIDENCE ANGLE BEGINS WITH AN INITIAL GUESS
c
 1    theta=atan(d/(h+z/eps))
      do 2 it=1,nit
      eta=1./sqrt(2.)*sqrt(eps+sin(theta)**2.+sqrt((eps-
     % sin(theta)**2.)**2.+(18.*sig/f)**2.))
      phi=asin(sin(theta)/eta)
 2    theta=atan((d-z*tan(phi))/h)
c
c     "nit" th ITERATION VALUES FOR THE INCIDENCE AND THE REFRACTION ANGLES
c     "theta" AND "phi" AND THE REFRACTIVE INDEX "eta" ARE TAKEN TO BE THEIR
c     SOLUTIONS.THEN THE LENGTHS OF THE AIR AND THE SUBSURFACE PARTS OF THE RAY
c     PATH FOLLOW
c
      d1=h/cos(theta)
      d2=z/cos(phi)
 3    return
      end
```

1.2 GENERAL INSTRUCTIONS AND COMMENTS

This is not a directly executable routine but a subroutine to be appended to the end of the main programs and called appropriately. It performs the most basic calculations required by our wave propagation model [1].

1.3 DESCRIPTION OF THE PROBLEM AND THE METHODS OF SOLUTION USED BY THE SUBROUTINE

The most basic calculation required by our wave propagation model is determining the lengths of the air and the subsurface parts of the total ray path between two given points (P_1 and P_2) located anywhere in a media composed of air and a subsurface medium, separated by a planar interface (each medium is homogeneous, isotropic, nonmagnetizable and conducting except for air, which is nonconducting,) i.e., calculating d_1 and d_2 shown in Figure 2.

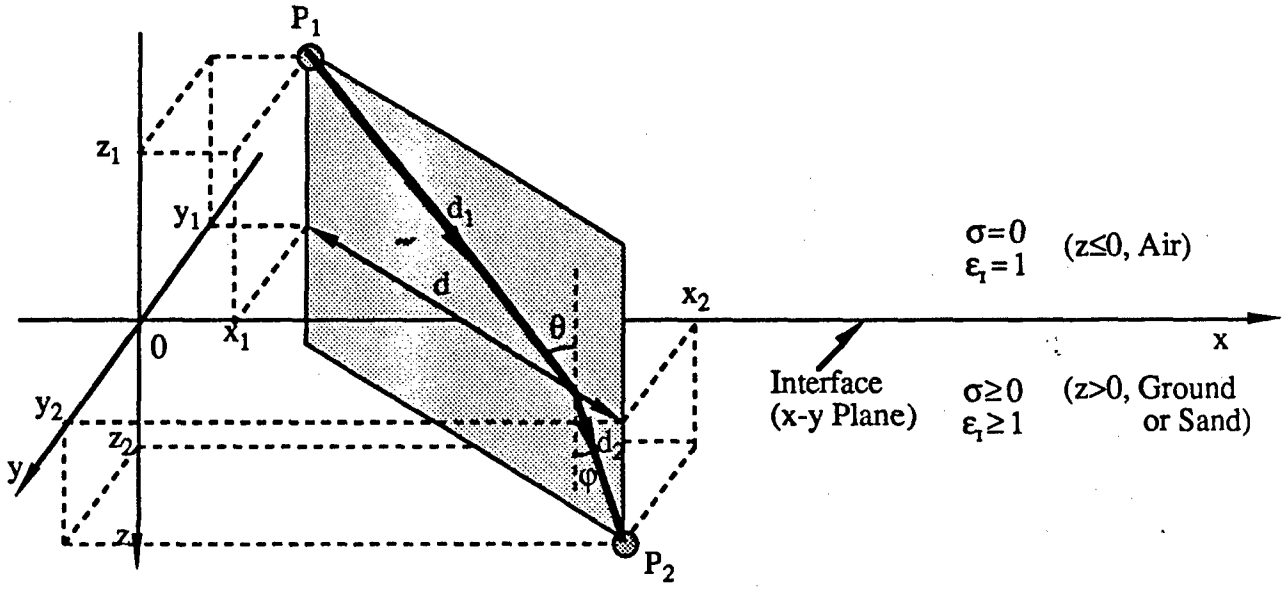

Figure 2: 3-D Ray Propagation Geometry

Although, at first, the problem looks like a 3-D problem, the propagation of the ray from P_1 to P_2 takes place in the incidence plane defined by the air and the subsurface parts

of the total ray path, and therefore, it is actually a 2-D problem. Then consider the planar geometry in Figure 3, where, with reference to Figure 2,

$$h = -z_1$$
$$z = z_2$$
$$d = \sqrt{(x_2 - x_1)^2 + (y_2 - y_1)^2}$$

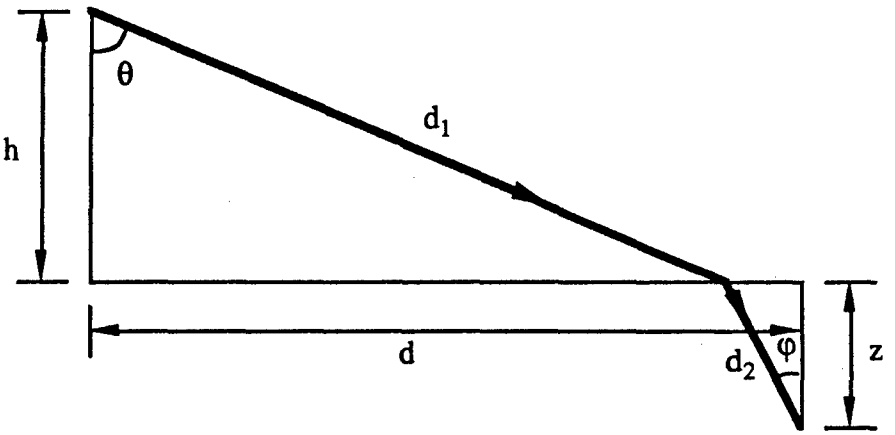

Figure 3: 2-D Ray Propagation Geometry

From the Snell's Law, we have

$$\mathrm{Sin}\varphi = \frac{\mathrm{Sin}\theta}{\eta(\theta)} \tag{1}$$

where

$$\eta(\theta) = \frac{1}{\sqrt{2}}\sqrt{\varepsilon_r + \mathrm{Sin}^2\theta + \sqrt{(\varepsilon_r - \mathrm{Sin}^2\theta)^2 + \left(\frac{18\sigma}{f}\right)^2}} \tag{2}$$

and is called the refractive index of the subsurface medium. ε_r and σ are the relative dielectric constant and the conductivity of the subsurface medium, respectively, and f is the frequency of radiation in units of GHz.

From the geometry in Figure 3,

$$d = h \tan\theta + z \tan\varphi \tag{3}$$

Substituting (1) in (3),

$$d = h \tan\theta + z \tan\left[\mathrm{Sin}^{-1}\left(\frac{\mathrm{Sin}\theta}{\eta(\theta)}\right)\right] \tag{4}$$

where the only unknown is the incidence angle θ. The difficulty of obtaining an analytical solution for θ from the last equation is surely appreciated. Then, we have searched for an iterative solution and come up with the following solution, which has been observed to converge quite fast: We start with a good initial guess, which we have determined, by trying, to be

$$\theta^{(0)} = \tan^{-1}\left(\frac{d}{h + z/\varepsilon_r}\right) \tag{5a}$$

Then using (1) and (3), we have the following iterations for φ and θ:

$$\varphi^{(n)} = \mathrm{Sin}^{-1}\left\{\frac{\mathrm{Sin}\theta^{(n-1)}}{\eta\left[\theta^{(n-1)}\right]}\right\} \tag{5b}$$

$$\theta^{(n)} = \tan^{-1}\left[\frac{d - z\tan\varphi^{(n)}}{h}\right] \quad , \quad n = 1,2,3,... \tag{5c}$$

where $\eta(\theta)$ is as given in (2).

For $z<50$ cm, θ converges reasonably close to the solution *in less than 5 iterations*. Having calculated φ and θ, d_1 and d_2 can be, from Figure 3, simply expressed as

$$d_1 = \frac{h}{\mathrm{Cos}\theta}$$

$$d_2 = \frac{z}{\mathrm{Cos}\varphi}$$

Also the refractive index $\eta(\theta)$ is readily computed from (2).

PROGRAM #2: *proptime.f*

Location: *ozdemir/research/proptime*

2.1 CODE

```
c     This program calculates the total propagation time of the wave from the
c     transmitter to each specified scan point and then from each scan point to
c     each specified receiver element in a media composed of air and a
c     conductive subsurface medium seperated by a planar interface. There is
c     only one transmitter element. Receiver array is periodic and oriented
c     parallel to one of x,y or z axes.
c
c     PARAMETERS AND VARIABLES USED IN THE PROGRAM
c
c     INPUT PARAMETERS:
c
c     eps: Relative dielectric constant of the subsurface medium (>=1)
c     sig: Conductivity of the subsurface medium [mho/meter]
c       f: Frequency of radiation [GHz]
c     nit: Number of iterations for subroutine "interface" to calculate the
c          incidence angle
c     nel: Number of elements of the receiver array
c    spel: Constant receiver element spacing [cm]
c     xrc: x-coordinate of the center of the receiver array [cm]
c     yrc: y                    "
c     zrc: z                    "
c     dir: direction (orientation) of the receiver array (x,y or z)
c     xtr: x-coordinate of the transmitter [cm]
c     ytr: y              "
c     ztr: z              "
c    z1sc: z-coordinate of the first scan point [cm]
c    z2sc:       "              last        "
c    dzsc: Spacing between the scan points in z direction [cm] (non zero)
c    y1sc: y-coordinate of the first scan point [cm]
c    y2sc:       "              last        "
c    dysc: Spacing between the scan points in y direction [cm] (non zero)
c    x1sc: x-coordinate of the first scan point [cm]
c    x2sc:       "              last        "
c    dxsc: Spacing between the scan points in x direction [cm] (non zero)
c          (If no scanning is desired in, for example, x direction, specify in
c           the input file x1sc=x2sc and dxsc=1)
c   fname: Name of the output file for storing the computed propagation times
c          (maximum 25 characters)
c
c     VARIABLES:
c
c     nzsc: Number of scan points in z direction
c     nysc:              "             y     "
c     nxsc:              "             z     "
c      zsc: z-coordinate of the current scan point [cm]
c      ysc: y                    "
c      xsc: x                    "
c      xel: x-coordinate of the current receiver element position [cm]
c      yel: y                                "
c      zel: z                                "
c      del: Distance of the current receiver element position to the center
c           of the receiver array [cm]
```

```
c       eta: Refractive index of the subsurface medium evaluated at the
c            incidence angle satisfying the ray geometry in transmit or receive
c            incidence plane
c        d1: Length of the air part of the ray path in transmit or receive
c            incidence plane
c        d2: Length of the subsurface part of the ray path in transmit or
c            receive incidence plane
c        t1: Propagation time in the transmit incidence plane [nsec]
c        t2:          "                receive          "
c         t: Total propagation time (t1 + t2) [nsec]
c
c
c
      dimension t(50)
      character*25 fname
      character dir
c
c     OPEN THE INPUT FILE "proptime.in" AND READ THE INPUT PARAMETERS
c     DESCRIBING THE IMAGING SET-UP AND THE MEDIA
c
      open(11,file='proptime.in')
      read(11,'(f10.4)') eps,sig,f
      read(11,'(i3)') nit,nel
      read(11,'(f10.4)') spel,xrc,yrc,zrc
      read(11,'(a)') dir
      read(11,'(f10.4)') xtr,ytr,ztr,z1sc,z2sc,dzsc,y1sc,y2sc,dysc,
     % x1sc,x2sc,dxsc
      read(11,'(a25)') fname
c
c     DETERMINING THE NUMBER OF SCAN POINTS IN z,y AND x DIRECTIONS
c
      nzsc=nint((z2sc-z1sc)/dzsc)+1
      nysc=nint((y2sc-y1sc)/dysc)+1
      nxsc=nint((x2sc-x1sc)/dxsc)+1
c
c     OPEN THE OUTPUT FILE FOR STORING THE PROPAGATION TIMES
c
      open(21,file=fname,status='new')
c
c     SPECIFYING THE LOCATIONS OF THE SCAN POINTS IN x,y and z DIRECTIONS
c
      do 1 ixsc=1,nxsc
         xsc=x1sc+dxsc*float(ixsc-1)
      do 1 izsc=1,nzsc
         zsc=z1sc+dzsc*float(izsc-1)
      do 1 iysc=1,nysc
         ysc=y1sc+dzsc*float(iysc-1)
c
c     CALCULATING THE LENGTHS OF THE AIR AND THE SUBSURFACE PARTS OF THE RAY
c     PATH FROM THE TRANSMITTER TO THE SCAN POINT
c
      call interface(eps,sig,f,xtr,ytr,ztr,xsc,ysc,zsc,nit,eta,d1,d2)
c
c     CALCULATING THE PROPAGATION TIME FROM THE TRANSMITTER TO THE SCAN POINT
c
      t1=(d1+eta*d2)/30.
c
c     SPECIFYING RECEIVER ELEMENT POSITIONS
c
      xel=xrc
      yel=yrc
      zel=zrc
      do 2 irc=1,nel
      del=spel*(float(irc)-float(nel+1)/2.)
      if(dir.eq.'x') xel=xrc+del
      if(dir.eq.'y') yel=yrc+del
```

```
      if(dir.eq.'z') zel=zrc+del
c
c     CALCULATING THE LENGTHS OF THE AIR AND THE SUBSURFACE PARTS OF THE RAY
c     PATH FROM THE SCAN POINT TO THE RECEIVER ELEMENT
c
      call interface(eps,sig,f,xsc,ysc,zsc,xel,yel,zel,nit,eta,d1,d2)
c
c     CALCULATING THE PROPAGATION TIME FROM THE SCAN POINT TO THE RECEIVER
c
      t2=(d1+eta*d2)/30.
c
c     CALCULATING THE TOTAL PROPAGATION TIME FROM THE TRANSMITTER TO THE
c     SCAN POINT AND FROM THERE TO THE RECEIVER
c
 2    t(irc)=t1+t2
c
c     WRITE INTO THE OUTPUT FILE THE TOTAL PROPAGATION TIMES FOR THE CURRENT
c     SCAN POINT
c
 1    write(21,'(8f9.5)') (t(irc),irc=1,nel)
      stop
      end
c
c     THIS SUBROUTINE CALCULATES THE LENGTHS OF THE AIR AND THE SUBSURFACE
c     PARTS OF THE RAY PATH BETWEEN TWO SEPERATE POINTS (P1 AND P2) IN A MEDIA
c     COMPOSED OF AIR AND A SUBSURFACE MEDIUM, EACH OF WHICH IS A HOMOGENOUS,
c     ISOTROPIC, NONMAGNETIZABLE AND CONDUCTING (EXCEPT FOR AIR, WHICH IS
c     NONCONDUCTING) MEDIUM, SEPERATED BY A PLANAR INTERFACE. THE POINTS CAN BE
c     IN DIFFERENT MEDIUMS AS WELL AS IN THE SAME MEDIUM. THE INTERFACE IS THE
c     Z=0 OR (X-Y) PLANE. POINTS WITH Z<=0 ARE IN THE AIR MEDIUM WHILE POINTS
c     WITH Z>0 ARE IN THE SUBSURFACE MEDIUM.
c
c
c     THE PARAMETERS AND THE VARIABLES USED IN THE CODE:
c
c     eps (INPUT PARAMETER) : RELATIVE DIELECTRIC CONSTANT OF THE SUBSURFACE
c                             MEDIUM (>=1)
c     sig (      "        ) : CONDUCTIVITY OF THE SUBSURFACE MEDIUM [mho/meter]
c     f   (      "        ) : FREQUENCY OF RADIATION [GHz]
c     x1  (      "        ) : X-COORDINATE OF THE FIRST POINT (P1) [cm]
c     y1  (      "        ) : Y-                  "
c     z1  (      "        ) : Z                   "
c     x2  (      "        ) : X-COORDINATE OF THE SECOND POINT (P2) [cm]
c     y2  (      "        ) : Y                   "
c     z2  (      "        ) : Z                   "
c     nit (      "        ) : NUMBER OF ITERATIONS IN CALCULATING THE INCIDENCE
c                             ANGLE
c     eta (OUTPUT PARAMETER): REFRACTIVE INDEX OF THE SUBSURFACE MEDIUM
c                             EVALUATED AT THE CALCULATED INCIDENCE ANGLE
c     d1  (      "         ): THE LENGTH OF THE AIR PART OF THE RAY PATH [cm]
c     d2  (      "         ): THE LENGTH OF THE SUBSURFACE PART OF THE RAY PATH
c                             [cm]
c     theta (INTERMEDIATE VARIABLE) : INCIDENCE ANGLE [rad]
c     phi   (          "          ) : REFRACTION ANGLE [rad]
c     d     (INTERMEDIATE PARAMETER): HORIZONTAL DISTANCE BETWEEN THE POINTS P1
c                                     AND P2 [cm]
c     h     (          "          ): HIGHT OF THE POINT (P1 OR P2) IN THE AIR
c                                     FROM THE INTERFACE [cm]
c     z     (          "          ): DEPTH OF THE POINT IN THE SUBSURFACE
c                                     MEDIUM FROM THE SURFACE (INTERFACE) [cm]
c
c
      subroutine interface(eps,sig,f,x1,y1,z1,x2,y2,z2,nit,eta,d1,d2)
      real eps,sig,f,x1,y1,z1,x2,y2,z2,eta,d1,d2
      integer nit
c
```

```
c     REDUCTION OF THE 3-D PROBLEM TO A PLANAR GEOMETRY PROBLEM
c
      d=sqrt((x1-x2)**2.+(y1-y2)**2.)
c
c     IF BOTH POINTS (P1 AND P2) ARE IN THE AIR MEDIUM OR eps=1....
c
      if((z1.le.0..and.z2.le.0.).or.eps.eq.1.) then
      d1=sqrt(d**2.+(z1-z2)**2.)
      d2=0.
      eta=1.
      goto 3
      end if
c
c     IF BOTH POINTS (P1 AND P2) ARE IN THE SUBSURFACE MEDIUM...
c
      if(z1.ge.0..and.z2.ge.0.) then
      d1=0.
      d2=sqrt(d**2.+(z1-z2)**2.)
      eta=1./sqrt(2.)*sqrt(eps+sqrt(eps**2.+(18.*sig/f)*2.))
      goto 3
      end if
c
c     IF THE POINTS ARE IN DIFFERENT MEDIA
c
      if(z1.le.0..and.z2.gt.0.) then
      h=-z1
      z=z2
      goto 1
      else
      h=-z2
      z=z1
      end if
c
c     ITERATION FOR THE INCIDENCE ANGLE BEGINS WITH AN INITIAL GUESS
c
 1    theta=atan(d/(h+z/eps))
      do 2 it=1,nit
      eta=1./sqrt(2.)*sqrt(eps+sin(theta)**2.+sqrt((eps-
     % sin(theta)**2.)**2.+(18.*sig/f)**2.))
      phi=asin(sin(theta)/eta)
 2    theta=atan((d-z*tan(phi))/h)
c
c     "nit" th ITERATION VALUES FOR THE INCIDENCE AND THE REFRACTION ANGLES
c     "theta" AND "phi" AND THE REFRACTIVE INDEX "eta" ARE TAKEN TO BE THEIR
c     SOLUTIONS.THEN THE LENGTHS OF THE AIR AND THE SUBSURFACE PARTS OF THE RAY
c     PATH FOLLOW
c
      d1=h/cos(theta)
      d2=z/cos(phi)
 3    return
      end
```

2.2 GENERAL INSTRUCTIONS AND COMMENTS

The program makes use of the previously described subroutine *interface.f* (in calculating the lengths of the refracted ray paths), which has been appended to the end of the program. It reads the input data from an input file called *proptime.in*.

To run this program on IBM PC, just change the extention of the program file name from "f" to "for", and follow the instructions given in the beginning of this report on running programs on IBM PC's.

The runing time of the program is roughly proportional to the number of scan points times the number of receiver elements. Let the number of scan points in longitudinal, vertical and horizontal directions be N_x, N_z, N_y, and the number of receiver elements be N_r, respectively. When N_x=1, N_z=51, N_y=101, N_r=22, the program took 126 minutes to run. Then the formula for runing time (on IBM PC) is

$$\text{Runing Time} \approx 126 \times (N_x \times N_z \times N_y \times N_r) / (1 \times 51 \times 101 \times 22) \text{ Minutes.}$$

2.2.1 INPUT FILE: *proptime.in*

Format:

Line #	Input Parameter	Format	Description of Parameter
1	eps	f10.4	Relative Dielectric Constant of the Subsurface Medium (≥1)
2	sig	"	Conductivity of the Subsurface Medium [mho/meter] (≥0)
3	f	"	Frequency of Radiation [GHz]
4	nit	i3	Number of Iterations for Subroutine "*interface*" to Calculate the Incidence Angle
5	nel	"	Number of Elements of the Receiver Array
6	spel	f10.4	Constant Receiver Element Spacing [cm]
7	xrc	"	x-Coordinate of the Center of the Receiver Array [cm]
8	yrc	"	y "
9	zrc	"	z "
10	dir	a	Direction of the Receiver Array: Put 'x' If Parallel to x Put 'y' " y

			Put 'z' " z
11	xtr	f10.4	x-Coordinate of the Transmitter [cm]
12	ytr	"	y "
13	ztr	"	z "
14	z1sc	"	z-Coordinate of the First Scan Point [cm]
15	z2sc	"	" Last "
16	dzsc	"	Spacing Between the Scan Points in z Direction [cm] ($\neq$0)
17	y1sc	"	y-Coordinate of the First Scan Point [cm]
18	y2sc	"	" Last "
19	dysc	"	Spacing Between the Scan Points in y Direction [cm] ($\neq$0)
20	x1sc	"	x-Coordinate of the First Scan Point [cm]
21	x2sc	"	" Last "
22	dxsc	"	Spacing Between the Scan Points in x Direction [cm] ($\neq$0) (If no scaning (imaging) is desired in, for example, x direction, specify in the input file x1sc=x2sc and dxsc=1cm)
23	fname	a25	Name of the Output File for Storing the Computed Propagation Times (maximum 25 characters)

2.3 DESCRIPTION OF THE PROBLEM AND THE METHODS OF SOLUTION USED BY THE PROGRAM

This program calculates the total propagation time of the wave from the transmitter location to each specified scan point and then from the scan point to each specified receiver position in a media composed of air and a conductive subsurface medium separated by a planar interface. Transmitter location and the scan points as well as the receiver positions can be specified in any medium (air or subsurface medium.) The restrictions are: The transmitter has one element, the scan points can span a 3-D space, and the receiver positions should be lined up parallel to one of x, y or z-axes. Consider the geometry in Figure 4.

As it is seen in Figure 4, the total propagation time consists of two parts. One in the *transmit incidence plane* and the other in the *receive incidence plane*. The geometry of the problem in each plane is basically the same as shown in Figure 2, where the problem was to compute the lengths of the air and the subsurface parts of the ray path, i.e., d_1 and d_2, which is exactly what the subroutine *interface.f* does. Then we can use this subroutine to

compute d_1 and d_2 in both *transmit and receive incidence planes*, and with the knowledge of the propagation speeds in each medium, which are determined by the relative dielectric constant (ε_r) and the conductivity (σ) of the respective medium through the refractive index, we can compute the total propagation time.

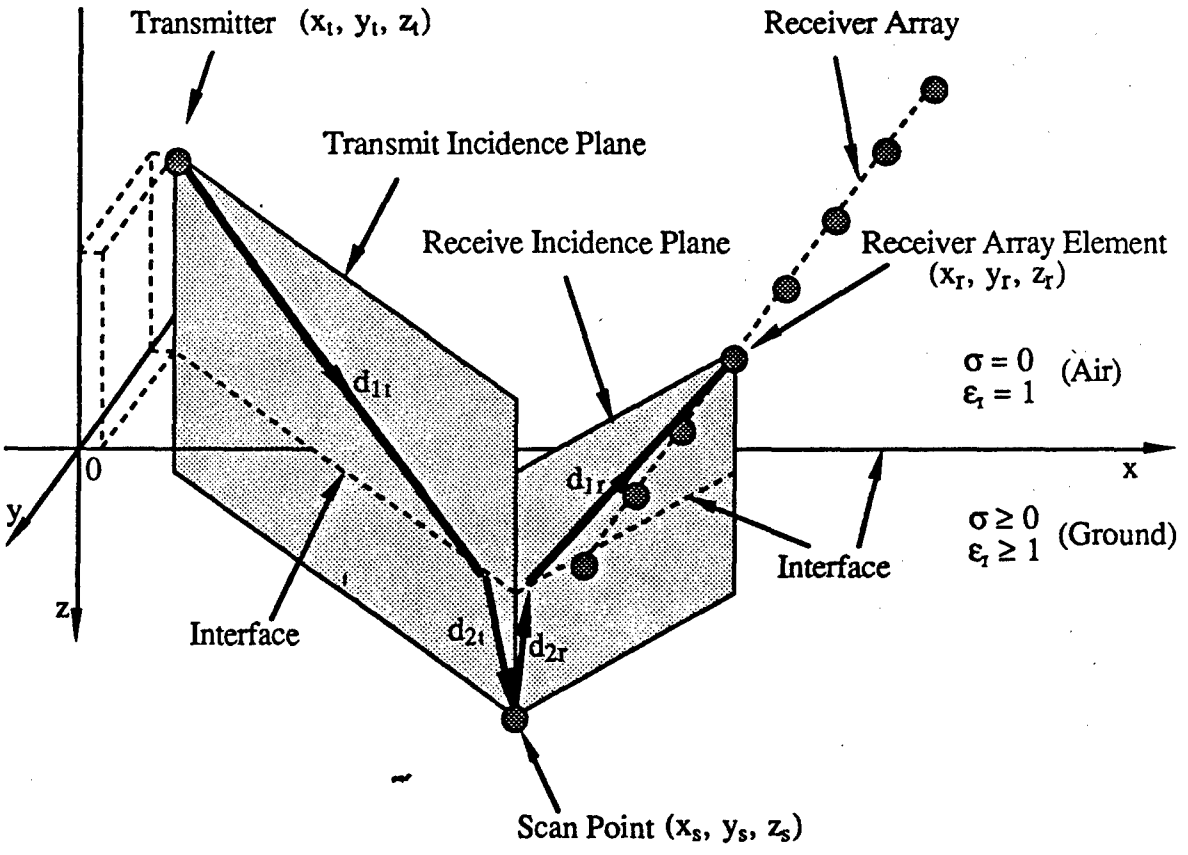

Figure 4: 3-D Ray Propagation Geometry

Let the lengths of the air and the subsurface parts of the ray path in the Transmit and Receive Incidence Planes be d_{1t} and d_{2t}, and d_{1r} and d_{2r}, and the subsurface propagation speeds be $c/\eta(\theta_t)$ and $c/\eta(\theta_r)$, respectively. c is the speed of light in free-space. $\eta(\theta_t)$ and $\eta(\theta_r)$ are the refractive indices of the subsurface medium evaluated at the incidence angles satisfying the ray geometry in Transmit and Receive Incidence Planes, respectively. Then the total propagation time from the transmitter to the receiver is

$$\tau = \frac{d_{1t}}{c} + \frac{d_{2t}}{\frac{c}{\eta(\theta_t)}} + \frac{d_{2r}}{\frac{c}{\eta(\theta_r)}} + \frac{d_{1r}}{c} \qquad (6)$$

This is repeated for each scan point and receiver position specified.

As long as the parameters and the geometry of the imaging setup remain constant, the propagation times will not change. Therefore, they need to be computed only once. After they are stored, they can be reused for imaging of different targets (by the program to be explained next) for which the I and Q data are collected with the same imaging setup.

PROGRAM #3: *image.f*

Location: *ozdemir/research/imaging*

3.1 CODE

```
c     THIS PROGRAM FORMS THE IMAGE OF A SPECIFIED TARGET REGION USING THE
c     PRE-CALCULATED PROPAGATION TIMES AND THE TIME SAMPLES OF THE INPHASE AND
c     THE QUADRATURE COMPONENTS OF THE COMPLEX WAVEFORMS MEASURED AT THE
c     OUTPUT OF THE RECEIVER ARRAY ELEMENTS. THE IMAGE FORMING IS PERFORMED IN
c     ACCORDANCE WITH THE IMAGING MODEL PRESENTED IN "VFRC PROGRESS REPORT NO.
c     59" (REFERENCE 1).
c
c
c     INPUT PARAMETERS:
c
c     nel: NUMBER OF RECEIVER ARRAY ELEMENTS
c     nsamp: NUMBER OF TIME SAMPLES OF THE I AND Q WAVEFORMS
c     nz: NUMBER OF SCAN POINTS IN z-DIRECTION
c     ny:              "            y     "
c     nx:              "            x     "
c     iref: THE SAMPLE NUMBER CORRESPONDING TO THE CENTER OF THE PULSE
c           SCATTERED FROM THE REFERENCE SCATTERING POINT AND MEASURED AT THE
c           REFERENCE MEASUREMENT POINT.
c     xtr: x-COORDINATE OF THE TRANSMITTER [cm]
c     ytr: y           "
c     ztr: z           "
c     xrs: x-COORDINATE OF THE REFERENCE SCATTERING POINT [cm]
c     yrs: y           "
c     zrs: z           "
c     xrm: x-COORDINATE OF THE REFERENCE MEASUREMENT POINT [cm]
c     yrm: y           "
c     zrm: z           "
c     eps: RELATIVE DIELECTRIC CONSTANT OF THE SUBSURFACE MEDIUM (>=1)
c     sig: CONDUCTIVITY OF THE SUBSURFACE MEDIUM [mho/meter] (>=0)
c     f: FREQUENCY OF RADIATION [GHz]
c     tsamp: SAMPLING TIME INTERVAL FOR I AND Q DATA [nsec]
c     iqname: NAME OF THE INPUT FILE CONTAINING THE MEASURED I AND Q DATA
c     tmname: NAME OF THE INPUT FILE CONTAINING THE COMPUTED PROPAGATION TIMES
c     imname: NAME OF THE OUTPUT FILE FOR STORING THE PRODUCED IMAGE DATA
c
c
c     VARIABLES:
c
c     in: INPHASE COMPONENT OF THE RECEIVED FIELD
c     qd: QUADRATURE COMPONENT OF THE RECEIVED FIELD
c     t1: PROPAGATION TIME FROM THE TRANSMITTER TO THE REFERENCE SCATTERER
c         POINT [nsec]
c     t2: PROPAGATION TIME FROM THE REFERENCE SCATTERER POINT TO THE REFERENCE
c         MEASUREMENT POINT [nsec]
c     tref: REFERENCE TOTAL PROPAGATION TIME FROM THE TRANSMITTER TO THE
c           REFERENCE MEASUREMENT POINT (t1 + t2) [nsec]
c     w: ANGULAR FREQUENCY OF RADIATION [rad/nsec]
c     t: TOTAL PROPAGATION TIME FROM THE TRANSMITTER TO THE SPECIFIED SCAN
c        POINT AND THEN TO THE SPECIFIED RECEIVE ARRAY ELEMENT POSITION [nsec]
c     isamp: SAMPLE NUMBER CORRESPONDING TO THE CENTER OF THE PULSE SCATTERED
c            FROM THE SPECIFIED SCAN POINT AND MEASURED AT THE SPECIFIED
c            RECEIVE ARRAY ELEMENT
```

```
c
      s(nx,nz,ny)=150.
c
c     OPEN THE OUTPUT FILE AND STORE THE IMAGE DATA
c
      open(51,file=imname)
      write(51,'(10li4)') (((nint(s(ix,iz,iy)),iy=1,ny),iz=1,nz),
     % ix=1,nx)
      stop
      end
c
c
c     THIS SUBROUTINE CALCULATES THE LENGTHS OF THE AIR AND THE SUBSURFACE
c     PARTS OF THE RAY PATH BETWEEN TWO SEPERATE POINTS (P1 AND P2) IN A MEDIA
c     COMPOSED OF AIR AND A SUBSURFACE MEDIUM, EACH OF WHICH IS A HOMOGENOUS,
c     ISOTROPIC, NONMAGNETIZABLE AND CONDUCTING (EXCEPT FOR AIR, WHICH IS
c     NONCONDUCTING) MEDIUM, SEPERATED BY A PLANAR INTERFACE. THE POINTS CAN BE
c     IN DIFFERENT MEDIUMS AS WELL AS IN THE SAME MEDIUM. THE INTERFACE IS THE
c     Z=0 OR (X-Y) PLANE. POINTS WITH Z<=0 ARE IN THE AIR MEDIUM WHILE POINTS
c     WITH Z>0 ARE IN THE SUBSURFACE MEDIUM.
c
c
c     THE PARAMETERS AND THE VARIABLES USED IN THE CODE:
c
c     eps (INPUT PARAMETER) : RELATIVE DIELECTRIC CONSTANT OF THE SUBSURFACE
c                             MEDIUM (>=1)
c     sig (      "        ) : CONDUCTIVITY OF THE SUBSURFACE MEDIUM [mho/meter]
c     f   (      "        ) : FREQUENCY OF RADIATION [GHz]
c     x1  (      "        ) : X-COORDINATE OF THE FIRST POINT (P1) [cm]
c     y1  (      "        ) : Y                    "
c     z1  (      "        ) : Z                    "
c     x2  (      "        ) : X-COORDINATE OF THE SECOND POINT (P2) [cm]
c     y2  (      "        ) : Y                    "
c     z2  (      "        ) : Z                    "
c     nit (      "        ) : NUMBER OF ITERATIONS IN CALCULATING THE INCIDENCE
c                             ANGLE
c     eta (OUTPUT PARAMETER): REFRACTIVE INDEX OF THE SUBSURFACE MEDIUM
c                             EVALUATED AT THE CALCULATED INCIDENCE ANGLE
c     d1  (      "         ): THE LENGTH OF THE AIR PART OF THE RAY PATH [cm]
c     d2  (      "         ): THE LENGTH OF THE SUBSURFACE PART OF THE RAY PATH
c                             [cm]
c     theta (INTERMEDIATE VARIABLE) : INCIDENCE ANGLE [rad]
c     phi   (          "          ) : REFRACTION ANGLE [rad]
c     d     (INTERMEDIATE PARAMETER): HORIZONTAL DISTANCE BETWEEN THE POINTS P1
c                                     AND P2 [cm]
c     h     (          "          ): HIGHT OF THE POINT (P1 OR P2) IN THE AIR
c                                     FROM THE INTERFACE [cm]
c     z     (          "          ): DEPTH OF THE POINT IN THE SUBSURFACE
c                                     MEDIUM FROM THE SURFACE (INTERFACE) [cm]
c
c
      subroutine interface(eps,sig,f,x1,y1,z1,x2,y2,z2,nit,eta,d1,d2)
      real eps,sig,f,x1,y1,z1,x2,y2,z2,eta,d1,d2
      integer nit
c
c     REDUCTION OF THE 3-D PROBLEM TO A PLANAR GEOMETRY PROBLEM
c
      d=sqrt((x1-x2)**2.+(y1-y2)**2.)
c
c     IF BOTH POINTS (P1 AND P2) ARE IN THE AIR MEDIUM OR eps=1
c
      if((z1.le.0..and.z2.le.0.).or.eps.eq.1.) then
      d1=sqrt(d**2.+(z1-z2)**2.)
      d2=0.
      eta=1.
      goto 3
```

```
      end if
c
c     IF BOTH POINTS (P1 AND P2) ARE IN THE SUBSURFACE MEDIUM...
c
      if(z1.ge.0..and.z2.ge.0.) then
      d1=0.
      d2=sqrt(d**2.+(z1-z2)**2.)
      eta=1./sqrt(2.)*sqrt(eps+sqrt(eps**2.+(18.*sig/f)*2.))
      goto 3
      end if
c
c     IF THE POINTS ARE IN DIFFERENT MEDIA
c
      if(z1.le.0..and.z2.gt.0.) then
      h=-z1
      z=z2
      goto 1
      else
      h=-z2
      z=z1
      end if
c
c     ITERATION FOR THE INCIDENCE ANGLE BEGINS WITH AN INITIAL GUESS
c
 1    theta=atan(d/(h+z/eps))
      do 2 it=1,nit
      eta=1./sqrt(2.)*sqrt(eps+sin(theta)**2.+sqrt((eps-
     % sin(theta)**2.)**2.+(18.*sig/f)**2.))
      phi=asin(sin(theta)/eta)
 2    theta=atan((d-z*tan(phi))/h)
c
c     "nit" th ITERATION VALUES FOR THE INCIDENCE AND THE REFRACTION ANGLES
c     "theta" AND "phi" AND THE REFRACTIVE INDEX "eta" ARE TAKEN TO BE THEIR
c     SOLUTIONS.THEN THE LENGTHS OF THE AIR AND THE SUBSURFACE PARTS OF THE RAY
c     PATH FOLLOW
c
      d1=h/cos(theta)
      d2=z/cos(phi)
 3    return
      end
```

3.2 GENERAL INSTRUCTIONS AND COMMENTS

This program processes the measured I and Q data with the computed propagation times to form the image of the specified target area. It reads three input files: First one, named *image.in*, contains parameters and the names of the two other input files. The second one contains the total propagation times computed by the program *proptime.f*. The third one contains the measured I and Q data. It also makes use of the subroutine *interface* in calculating the reference propagation time for calibration purposes.

The IBM PC version of this program is the PROGRAM #4 to be described next.

3.2.1 INPUT FILE #1: *image.in*

This input file contains the input parameters and the names of the two other input files.

Format:

Line #	Input Parameter	Format	Description of the Parameter
1	nel	i3	Number of Receiver Array Elements
2	nsamp	"	Number of Samples of the I and Q waveforms
3	nz	"	Number of Scan Points in z Direction
4	ny	"	" y "
5	nx	"	" x " (if no scanning is desired in x direction, enter nx=1)
6	iref	i3	The sample number corresponding to the center of the pulse scattered from the reference scattering point and measured at the reference measurement point.
7	xtr	f10.4	x-Coordinate of the transmitter [cm]
8	ytr	"	y "
9	ztr	"	z "
10	xrs	"	x-Coordinate of the reference scattering point [cm]
11	yrs	"	y "
12	zrs	"	z "
13	xrm	"	x-Coordinate of the reference measurement point [cm]

14	yrm	"	y "
15	zrm	"	z "
16	eps	"	Relative dielectric constant of the subsurface medium (≥1)
17	sig	"	Conductivity of the subsurface medium [mho/meter] (≥0)
18	f	"	Frequency of radiation [GHz]
19	tsamp	"	Sampling time interval for I and Q data [nsec]
20	iqname	a25	Name of the input file containing the measured I and Q data
21	tmname	"	Name of the input file containing the computed propagation times
22	imname	"	Name of the output file for storing the image data

3.2.2 INPUT FILE #2: *(to be named by the user)*

This input file contains the Inphase (I) and Quadrature (Q) components of the measured complex waveforms at the output of the receiver array elements.

Format:

Starting with the first receiver element, for each receiver element, five I&Q pairs per line (ten numbers per line), each number is a five digit integer including its sign. First the inphase (I) then the quadrature (Q) component of the pair is stored. There are 500 I&Q pair samples for each receiver element.

3.2.3 INPUT FILE #3: *(to be named by the user)*

This input file contains the propagation times which have already been computed by the program *proptime.f* for the given imaging setup and the media.

Format:

Format of the data can be easily acquired from the code of the previously discussed program *proptime.f*. For each scan point, as many propagation times as the number of receiver elements are stored in as many lines of the input file as they can fill. Each line

contains eight numbers except for the last one which may contain less. For the next scan point the storing starts from the beginning of the next blank line. Numbers are stored in a floating number space with format "f9.5".

3.2 DESCRIPTION OF IMAGE PROCESSING

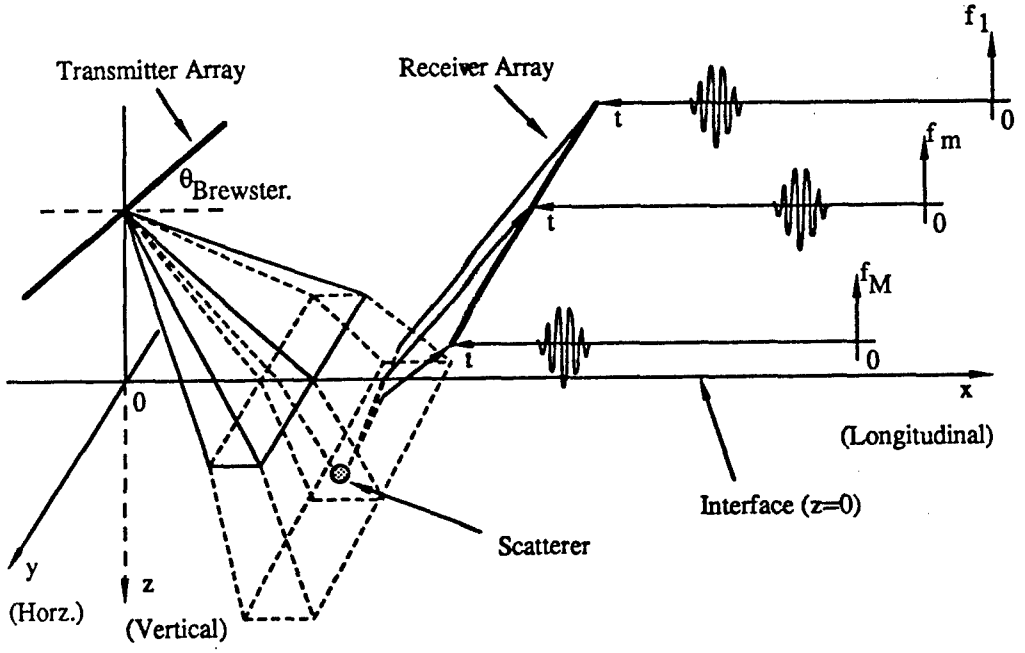

Figure 5: Imaging Geometry

Consider Figure 5 which shows the transmitter beam illuminating a strip on the ground. Let there be N isotropic (energy scattered uniformly in all directions) point scatterers within this volume. Each scatterer reradiates a portion of the incident wave (i.e. acts as the center of a propagating spherical wave front), and whose action is represented by an amplitude scattering coefficient R_n and a time-delay T_n of the incident pulse, n = 1, 2, ..., N. The receiver array consists of M elements and $f_m(t)$ represents the received field amplitude at the m^{th} receiver array element. The transmitted pulse is assumed to be as given in Figure 6 where the envelope is modelled to be Gaussian (to represent the band-limiting effect of the hardware on the ideal square pulse), the angular radiation frequency is ω and the effective pulse duration (spacing between 3 dB drop points) is T. Then the transmitted pulse can be expressed as

$$E(t) = \mathrm{Exp}\left[-(\ln 4)\left(\frac{t}{T}\right)^2\right]\mathrm{Cos}(\omega t) \qquad (7)$$

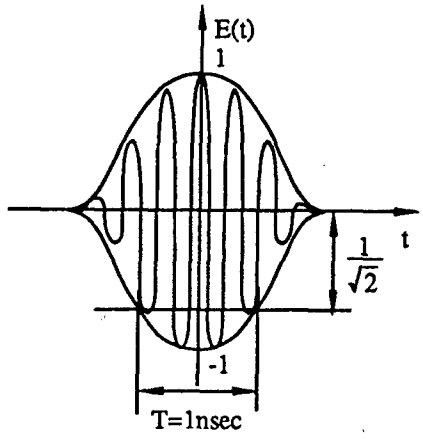

Figure 6: Transmitted Pulse

Further assume that the point scatterers cause no differential envelope delay during the process of scattering, and that the pulses arrive at the receiver without dispersion. Then, using (7) and the homogeneity of the medium, we can express the received real signal at the output of the m^{th} element as

$$f_m(t) = \sum_{n=1}^{N} R_n \,\mathrm{Exp}\left[-(\ln 4)\left(\frac{t-\tau_{nm}}{T}\right)^2\right]\mathrm{Cos}\left[\omega\left(t - T_n - \tau_{nm}\right)\right], \; m = 1, 2, \ldots, M \qquad (8)$$

where

R_n: Real scattering coefficient of the n^{th} scatterer.

τ_{nm}: Total propagation time from the transmitter to the m^{th} receiver element via the n^{th} scatterer.

T_n: Amount of time delay of the sinusoid of the pulse upon being scattered by the n^{th} scatterer.

ω: Carrier angular frequency.

The received signal $f_m(t)$ is a bandpass signal which can be represented by

$$f_m(t) = a_m(t)\,\mathrm{Cos}\left[\omega t - \varphi_m(t)\right] \qquad (9)$$

which is a sinusoidal signal with an angular frequency ω, and time-variant amplitude and phase. Then let us define complex analytical signal as

$$f_m^c(t) = a_m(t) \exp[i\varphi_m(t)] \tag{10}$$

which contains the same information as $f_m(t)$ does (i.e., amplitude and phase information.) Mathematically, it is alright to write (10) as

$$f_m^c(t) = a_m(t)\, \mathrm{Cos}[\varphi_m(t)] + i\, a_m(t)\, \mathrm{Sin}[\varphi_m(t)] \tag{11}$$

The signal that we measure as voltage at the output of the m^{th} receiver antenna is the real signal $f_m(t)$ represented in (9). If we expand the Cosine function in (9), we get

$$f_m(t) = \left\{a_m(t)\, \mathrm{Cos}[\varphi_m(t)]\right\} \mathrm{Cos}(\omega t) - \left\{a_m(t)\, \mathrm{Sin}[\varphi_m(t)]\right\} \mathrm{Sin}(\omega t) \tag{12}$$

Let
$$I_m(t) = a_m(t)\, \mathrm{Cos}[\varphi_m(t)] \tag{13a}$$

and
$$Q_m(t) = a_m(t)\, \mathrm{Sin}[\varphi_m(t)] \tag{13b}$$

Then
$$f_m(t) = I_m(t)\, \mathrm{Cos}(\omega t) - Q_m(t)\, \mathrm{Sin}(\omega t) \tag{14}$$

These new functions $I_m(t)$ and $Q_m(t)$ are called the *inphase* and the *quadrature* components, respectively, of the real signal $f_m(t)$. From (11) and (13a,b), we see that that $I_m(t)$ and $Q_m(t)$ are also the real and the imaginary parts of the complex analytical signal $f_m^c(t)$. That is, the inphase and the quadrature components of a real bandpass signal are the real and the imaginary parts, respectively, of its complex signal equivalent which contains all the necessary information about the real bandpass signal.

Then, in order to represent the measured signal (assumed to be bandpass) in a complex signal form, all we need to do is measure the I and Q components of the signal. From (14), we see that to get I and Q, we can multiply the real signal with the reference signals $\mathrm{Cos}(\omega t)$ and $\mathrm{Sin}(\omega t)$, respectively, and then low pass filter to get rid of the signals with 2ω frequency. After measuring I and Q components, using (12) and (13a,b), the received complex signal is

$$f_m^c(t) = I_m(t) + i\, Q_m(t)\,, \quad m=1,2,\ldots,M \tag{15}$$

Imaging the scatterers means estimating the real scattering coefficients R_n, n=1,2,..,N by processing the measured signals $f_m^c(t)$, m=1,2,..,M. How the information about the scattering coefficients are contained in the measurements is given to us by our modeling of the received signal in (8). Since it is already in the form of (9), its complex equivalent signal can be readily written as

$$f_m^c(t) = \sum_{n=1}^{N} R_n \, Exp\left[-(\ln 4)\left(\frac{t-\tau_{nm}}{T}\right)^2\right] \exp\left[i\omega(T_n+\tau_{nm})\right] \quad , m=1, 2,..., M \qquad (16)$$

Define a complex scattering coefficient S_n for the n^{th} scatterer as

$$S_n = R_n \exp(i\omega T_n)$$

Then, (16) becomes

$$f_m^c(t) = \sum_{n=1}^{N} \left\{ S_n \exp\left[-(\ln 4)\left(\frac{t-\tau_{nm}}{T}\right)^2\right]\right\} \exp(i\omega\tau_{nm}) \, , \quad m = 1, 2,..., M \qquad (17)$$

The goal of the image reconstruction process is to obtain "good" estimates of S_n, n=1,2,...,N, from the measurements $f^c{}_m(t)$, m=1,2,..,M. A suitable candidate is the simple "delay and sum" beamformer as argued below. Assume that we want to image the point (x_o,y_o,z_o) where the $n_o{}^{th}$ point scatterer is located, i.e., we wish to estimate S_{n_o} in the presence of other scatterers. Then, $f^c{}_m(t=\tau_{n_o m})$ will tend to have higher contribution from S_{n_o} compared to $f^c{}_m(t\neq\tau_{n_o m})$ as can be seen by writing

$$f_m^c(t=\tau_{n_o m}) = S_{n_o} \exp(i\omega\tau_{n_o m}) + \sum_{n\neq n_o} S_n \exp\left[-(\ln 4)(\tau_{n_o m}-\tau_{nm})^2\right] \exp(i\omega\tau_{nm}) \qquad (18)$$

for m = 1, 2,..., M.

A simple and obvious choice of an estimate of S_{n_o} from (18), is

$$\overline{S}_{n_o} = \frac{1}{M}\sum_{m=1}^{M} f_m^c(\tau_{n_o m}) \exp(-i\omega\tau_{n_o m}) \quad , n_o = 1, 2,..., N \qquad (19)$$

Since we have access to the I and Q components of the measurements $f^c_m(t)$, m=1,2,..,M, we should rewrite (19) as

$$\bar{S}_{n_o} = \frac{1}{M}\sum_{m=1}^{M}\left[I_m(\tau_{n_o m}) + i\,Q_m(\tau_{n_o m})\right]\exp(-i\,\omega\tau_{n_o m}) \qquad (20)$$

and

$$\bar{R}_{n_o} = \left|\bar{S}_{n_o}\right|$$

There is one problem in practice. To estimate S_{n_o}, we pick the best candidates as $f^c_m(t=\tau_{n_o m})$, m=1,2,...,M. In doing it, we argued that these numbers have higher contribution from S_{n_o} compared to $f^c_m(t\neq\tau_{n_o m})$ since, according to the model, the pulse coming from the n_o^{th} point scatterer peaks at $t=\tau_{n_o m}$. However, this is based on the assumption (in the model) that the peak of the pulse leaves the transmitter at t = 0. One might argue that this is alright since as long as we know the relative start time of the measurements with respect to the firing time of the transmitter. However, in practice, measurement of this relative time is not realistic and practical.

Instead, we have a more secure way around this problem. First of all, we keep the starting time of the sampling constant relative to the firing of the transmitter (which is unknown). We put a reference target (a metal plate) on the surface and look at the amplitude waveform of the received signal at the output of one of the receive array elements. Then, we locate in the time axis where the pulse from the reference target peaks and call it t_{ref} ("iref" in the program *image.f*). Next, we calculate the total propagation time of the same pulse from the transmitter to the receiver via the reference target and call it τ_{ref} ("tref" in the program). Then we have to add to every total propagation time τ_{nm} the amount $t_{ref}-\tau_{ref}$ in order to locate the pulses in the measured signals correctly. Considering this correction for the calculated propagation times, (20) takes the final form

$$\bar{R}_{n_o} = \left|\bar{S}_{n_o}\right| = \frac{1}{M}\left|\sum_{m=1}^{M}\left[I_m(t_{ref}+\tau_{n_o m}-\tau_{ref}) + i\,Q_m(t_{ref}+\tau_{n_o m}-\tau_{ref})\right]\exp(-i\omega\tau_{n_o m})\right|$$

We did not add the time correction to the phase term since the error in phase shifting term will remain constant for all m=1,2,...,M, and can be taken to the front of the summation, and therefore,will not effect the absolute value of the summation.

PROGRAM #4 (IBM PC Version) : *image.for*

Location: *ozdemir/research/ibm*

4.1 CODE

```
c
c
c     ****************************************************************
c     ******************** IBM VERSION ***********************************
c     ****************************************************************
c
c
c     THIS PROGRAM FORMS THE IMAGE OF A SPECIFIED TARGET REGION USING THE
c     PRE-CALCULATED PROPAGATION TIMES AND THE TIME SAMPLES OF THE INPHASE AND
c     THE QUADRATURE COMPONENTS OF THE COMPLEX WAVEFORMS MEASURED AT THE
c     OUTPUT OF THE RECEIVER ARRAY ELEMENTS. THE IMAGE FORMING IS PERFORMED IN
c     ACCORDANCE WITH THE IMAGING MODEL PRESENTED IN "VFRC PROGRESS REPORT NO.
c     59" (REFERENCE 1).
c
c
c     INPUT PARAMETERS:
c
c     nel: NUMBER OF RECEIVER ARRAY ELEMENTS
c     nsamp: NUMBER OF TIME SAMPLES OF THE I AND Q WAVEFORMS
c     nz: NUMBER OF SCAN POINTS IN z-DIRECTION
c     ny:              "              y     "
c     nx:              "              x     "
c     iref: THE SAMPLE NUMBER CORRESPONDING TO THE CENTER OF THE PULSE
c           SCATTERED FROM THE REFERENCE SCATTERING POINT AND MEASURED AT THE
c           REFERENCE MEASUREMENT POINT.
c     xtr: x-COORDINATE OF THE TRANSMITTER [cm]
c     ytr: y           "          "
c     ztr: z           "
c     xrs: x-COORDINATE OF THE REFERENCE SCATTERING POINT [cm]
c     yrs: y           "
c     zrs: z           "
c     xrm: x-COORDINATE OF THE REFERENCE MEASUREMENT POINT [cm]
c     yrm: y           "
c     zrm: z           "
c     eps: RELATIVE DIELECTRIC CONSTANT OF THE SUBSURFACE MEDIUM (>=1)
c     sig: CONDUCTIVITY OF THE SUBSURFACE MEDIUM [mho/meter] (>=0)
c     f: FREQUENCY OF RADIATION [GHz]
c     tsamp: SAMPLING TIME INTERVAL FOR I AND Q DATA [nsec]
c     iqname: NAME OF THE INPUT FILE CONTAINING THE MEASURED I AND Q DATA
c     tmname: NAME OF THE INPUT FILE CONTAINING THE COMPUTED PROPAGATION TIMES
c     imname: NAME OF THE OUTPUT FILE FOR STORING THE PRODUCED IMAGE DATA
c
c
c     VARIABLES:
c
c     in: INPHASE COMPONENET OF THE RECEIVED FIELD
c     qd: QUADRATURE COMPONENET OF THE RECEIVED FIELD
c     t1: PROPAGATION TIME FROM THE TRANSMITTER TO THE REFERENCE SCATTERER
c         POINT [nsec]
c     t2: PROPAGATION TIME FROM THE REFERENCE SCATTERER POINT TO THE REFERENCE
c         MEASUREMENT POINT [nsec]
c     tref: REFERENCE TOTAL PROPAGATION TIME FROM THE TRANSMITTER TO THE
```

```
c            REFERENCE MEASUREMENT POINT (t1 + t2) [nsec]
c      w: ANGULAR FREQUENCY OF RADIATION [rad/nsec]
c      t: TOTAL PROPAGATION TIME FROM THE TRANSMITTER TO THE SPECIFIED SCAN
c         POINT AND THEN TO THE SPECIFIED RECEIVE ARRAY ELEMENT POSITION [nsec]
c      isamp: SAMPLE NUMBER CORRESPONDING TO THE CENTER OF THE PULSE SCATTERED
c             FROM THE SPECIFIED SCAN POINT AND MEASURED AT THE SPECIFIED
c             RECEIVE ARRAY ELEMENT
c      s: ESTIMATE OF THE REAL SCATTERING COEFFICIENT OF THE SCATTERER ASSUMED
c         TO BE AT THE SPECIFIED SCAN POINT (VALUE OF THE PRODUCED GRAY SCALE
c         IMAGE AT THE SPECIFIED SCAN POINT)
c
c
      dimension t(22),s(101)
      integer in(22,301),qd(22,301),injunk,qdjunk
      complex sum
      character*25 iqname,tmname,imname
c
c     OPEN THE INPUT FILE
c
      open(11,file='image.in')
c
c     READ THE INPUT FILE
c
      read(11,'(i3)') nel,nsamp,nz,ny,nx
      read(11,'(i3)') iref
      read(11,'(f10.4)') xtr,ytr,ztr,xrs,yrs,zrs,xrm,yrm,zrm,eps,sig,
     % f,tsamp
      read(11,'(a25)') iqname,tmname,imname
c
c     CALCULATE THE TOTAL PROPAGATION TIME FROM THE TRANSMITTER TO THE
c     REFERENCE MEASUREMENT POINT VIA REFERENCE SCATTERING POINT
c
      call interface(eps,sig,f,xtr,ytr,ztr,xrs,yrs,zrs,10,eta,d1,d2)
      t1=(d1+eta*d2)/30.
      call interface(eps,sig,f,xrs,yrs,zrs,xrm,yrm,zrm,10,eta,d1,d2)
      t2=(d1+eta*d2)/30.
      tref=t1+t2
      w=8.*atan(1.)*f
c
c     OPEN THE INPUT FILES FOR PROPAGATION TIME AND IQ DATA, AND THE OUTPUT
c     FILE FOR STORING THE IMAGE DATA
c
      open(21,file=tmname)
      open(31,file=iqname)
c
c     READ THE IQ INPUT FILE
c
      do 6 i=1,22
6       read(31,'(10i5)') (injunk,qdjunk,j=1,199),
     % (in(i,j),qd(i,j),j=1,301)
      open(41,file=imname,status='new')
c
c     START FORMING THE IMAGE
c
      do 3 ix=1,nx
      do 3 iz=1,nz
      do 4 iy=1,ny
c
c     READ THE PROPAGATION TIMES THAT TAKE THE WAVE TO TRAVEL FROM THE
c     TRANSMITTER TO ALL THE RECEIVER ELEMENTS VIA THE SPECIFIED SCAN POINT
c
      read(21,'(8f9.5)') (t(iel),iel=1,nel)
      sum=cmplx(0.,0.)
c
c     PHASE SHIFTING AND SUMMING OVER RECEIVER ELEMENTS
c
```

```
      do 5 iel=1,nel
         isamp=iref+nint((t(iel)-tref)/tsamp)
         if(isamp.gt.nsamp) isamp=nsamp
 5       sum=sum+cmplx(float(in(iel,isamp-199)),
     % float(qd(iel,isamp-199)))*cexp(cmplx(0.,-w*t(iel)))
 4    s(iy)=cabs(sum)/float(nel)
c
c     ASSIGN TO THE CORNER OF THE IMAGE THE NORMALIZATION VALUE
c
      if(iz.eq.nz.and.ix.eq.nx) s(ny)=150.
 3    write(41,'(101i4)') (nint(s(iy)),iy=1,ny)
      stop
      end
c
c
c     THIS SUBROUTINE CALCULATES THE LENGTHS OF THE AIR AND THE SUBSURFACE
c     PARTS OF THE RAY PATH BETWEEN TWO SEPERATE POINTS (P1 AND P2) IN A MEDIA
c     COMPOSED OF AIR AND A SUBSURFACE MEDIUM, EACH OF WHICH IS A HOMOGENOUS,
c     ISOTROPIC, NONMAGNETIZABLE AND CONDUCTING (EXCEPT FOR AIR, WHICH IS
c     NONCONDUCTING) MEDIUM, SEPERATED BY A PLANAR INTERFACE. THE POINTS CAN BE
c     IN DIFFERENT MEDIUMS AS WELL AS IN THE SAME MEDIUM. THE INTERFACE IS THE
c     Z=0 OR (X-Y) PLANE. POINTS WITH Z<=0 ARE IN THE AIR MEDIUM WHILE POINTS
c     WITH Z>0 ARE IN THE SUBSURFACE MEDIUM.
c
c
c     THE PARAMETERS AND THE VARIABLES USED IN THE PROGRAM:
c
c     eps (INPUT PARAMETER) : RELATIVE DIELECTRIC CONSTANT OF THE SUBSURFACE
c                             MEDIUM (>=1)
c     sig (       "       ) : CONDUCTIVITY OF THE SUBSURFACE MEDIUM [mho/meter]
c     f   (       "       ) : FREQUENCY OF RADIATION [GHz]
c     x1  (       "       ) : X-COORDINATE OF THE FIRST POINT (P1) [cm]
c     y1  (       "       ) : Y                    "
c     z1  (       "       ) : Z                    "
c     x2  (       "       ) : X-COORDINATE OF THE SECOND POINT (P2) [cm]
c     y2  (       "       ) : Y                    "
c     z2  (       "       ) : Z                    "
c     nit (       "       ) : NUMBER OF ITERATIONS IN CALCULATING THE INCIDENCE
c                             ANGLE
c     eta (OUTPUT PARAMETER): REFRACTIVE INDEX OF THE SUBSURFACE MEDIUM
c                             EVALUATED AT THE CALCULATED INCIDENCE ANGLE
c     d1  (       "       ): THE LENGTH OF THE AIR PART OF THE RAY PATH [cm]
c     d2  (       "       ): THE LENGTH OF THE SUBSURFACE PART OF THE RAY PATH
c                             [cm]
c     theta (INTERMEDIATE VARIABLE) : INCIDENCE ANGLE [rad]
c     phi   (         "           ) : REFRACTION ANGLE [rad]
c     d     (INTERMEDIATE PARAMETER): HORIZONTAL DISTANCE BETWEEN THE POINTS P1
c                                     AND P2 [cm]
c     h     (         "           ): HIGHT OF THE POINT (P1 OR P2) IN THE AIR
c                                     FROM THE INTERFACE [cm]
c     z     (         "           ): DEPTH OF THE POINT IN THE SUBSURFACE
c                                     MEDIUM FROM THE SURFACE (INTERFACE) [cm]
c
c
      subroutine interface(eps,sig,f,x1,y1,z1,x2,y2,z2,nit,eta,d1,d2)
      real eps,sig,f,x1,y1,z1,x2,y2,z2,eta,d1,d2
      integer nit
c
c     REDUCTION OF THE 3-D PROBLEM TO A PLANAR GEOMETRY PROBLEM
c
      d=sqrt((x1-x2)**2.+(y1-y2)**2.)
c
c     IF BOTH POINTS (P1 AND P2) ARE IN THE AIR MEDIUM OR eps=1
c
      if((z1.le.0..and.z2.le.0.).or.eps.eq.1.) then
      d1=sqrt(d**2.+(z1-z2)**2.)
```

```
      d2=0.
      eta=1.
      goto 3
      end if
c
c     IF BOTH POINTS (P1 AND P2) ARE IN THE SUBSURFACE MEDIUM...
c
      if(z1.ge.0..and.z2.ge.0.) then
      d1=0.
      d2=sqrt(d**2.+(z1-z2)**2.)
      eta=1./sqrt(2.)*sqrt(eps+sqrt(eps**2.+(18.*sig/f)*2.))
      goto 3
      end if
c
c     IF THE POINTS ARE IN DIFFERENT MEDIA
c
      if(z1.le.0..and.z2.gt.0.) then
      h=-z1
      z=z2
      goto 1
      else
      h=-z2
      z=z1
      end if
c
c     ITERATION FOR THE INCIDENCE ANGLE BEGINS WITH AN INITIAL GUESS
c
 1    theta=atan(d/(h+z/eps))
      do 2 it=1,nit
      eta=1./sqrt(2.)*sqrt(eps+sin(theta)**2.+sqrt((eps-
     % sin(theta)**2.)**2.+(18.*sig/f)**2.))
      phi=asin(sin(theta)/eta)
 2    theta=atan((d-z*tan(phi))/h)
c
c     "nit" th ITERATION VALUES FOR THE INCIDENCE AND THE REFRACTION ANGLES
c     "theta" AND "phi" AND THE REFRACTIVE INDEX "eta" ARE TAKEN TO BE THEIR
c     SOLUTIONS.THEN THE LENGTHS OF THE AIR AND THE SUBSURFACE PARTS OF THE RAY
c     PATH FOLLOW
c
      d1=h/cos(theta)
      d2=z/cos(phi)
 3    return
      end
```

4.2 GENERAL INSTRUCTIONS AND COMMENTS

This program is the modified version of PROGRAM #3 to meet the memory allocation requirements of IBM PCs. Every thing else is exactly the same as for PROGRAM #3 (input, output files, formats, etc.)

The runing time of the program is roughly proportional to the number of scan points times the number of receiver elements. Let the number of scan points in longitudinal, vertical and horizontal directions be N_x, N_z, N_y, and the number of receiver elements be N_r, respectively. When N_x=1, N_z=51, N_y=101 and N_r=22, the program took 14.5 minutes to run. Then the formula for runing time (on IBM PC) is

$$\text{Runing Time} \approx 14.5 \times (N_x \times N_z \times N_y \times N_r) / (1 \times 51 \times 101 \times 22) \text{ Minutes.}$$

REFERENCES

[1] T. Özdemir, S. Roy, R.S. Berkowitz, "Applications of Subsurface Radar For Mine Detection," Valley Forge Research Center Quarterly Progress Report No.59, pp.20-39, October 1989 - March 1990.

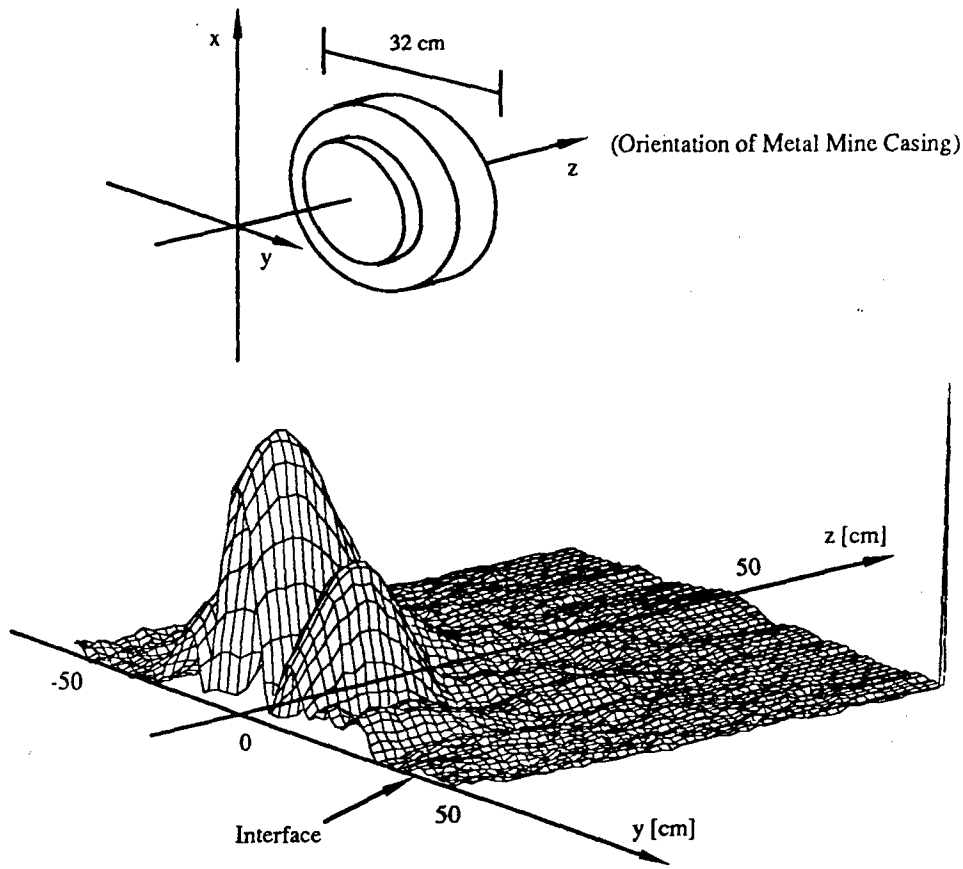

Figure 1 : Isometric Image of Metal Mine Casing 3" (7.5 cm) Below the Surface
ε_r =3.2, σ = 0.005 Date: 12/06/89

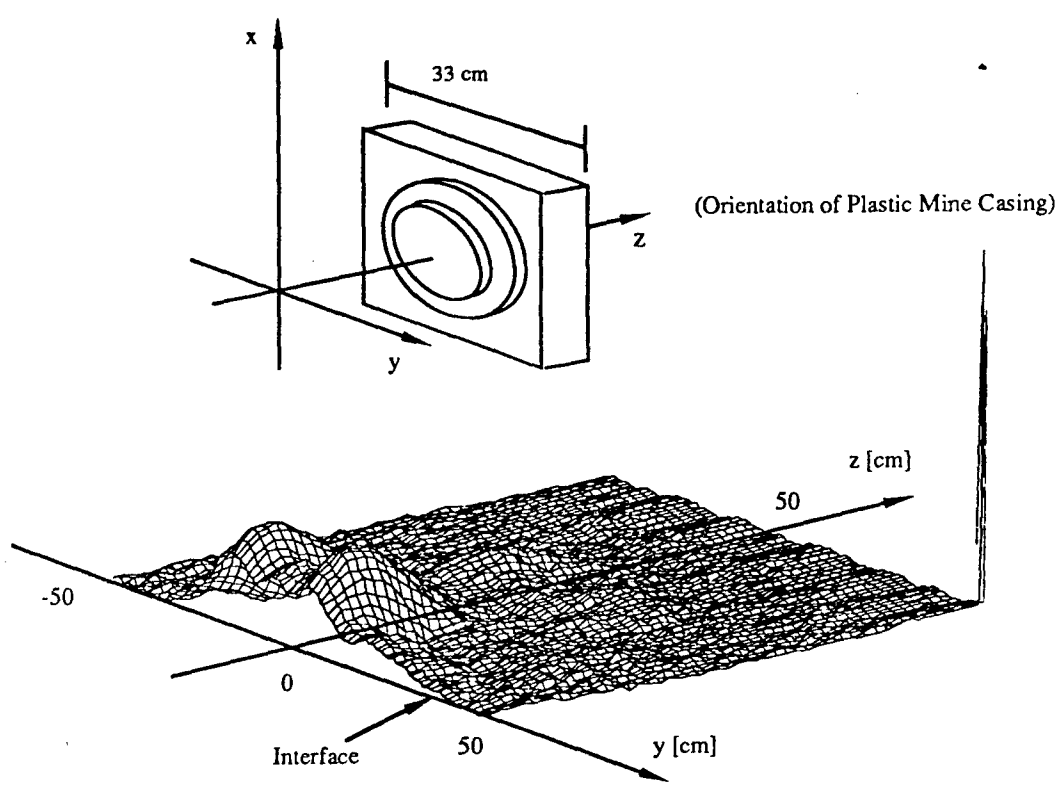

Figure 2 : Isometric Image of Plastic Mine 3" (7.5 cm) Below the Surface
ε_r = 3.2, σ = 0.005 Date: 12/06/89

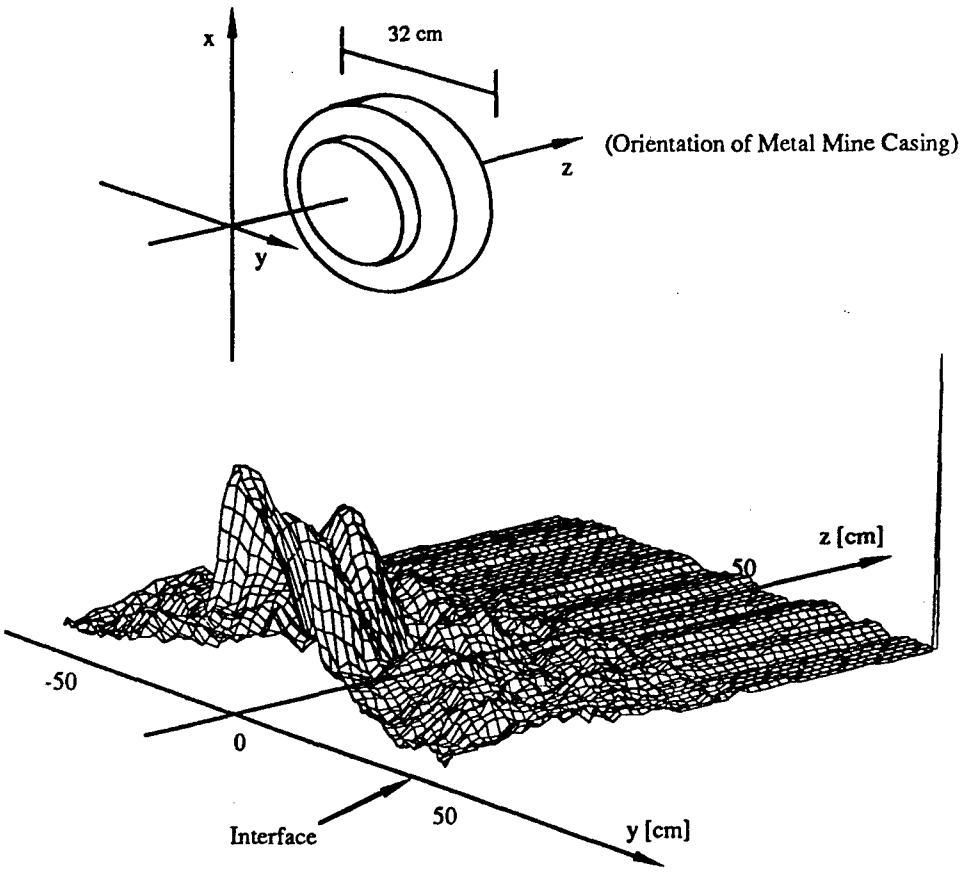

Figure 3 : Isometric Image of Metal Mine Casing 3" (7.5 cm) Below the Surface
ε_r =5.5, σ = 0.145 Date 08/01/90

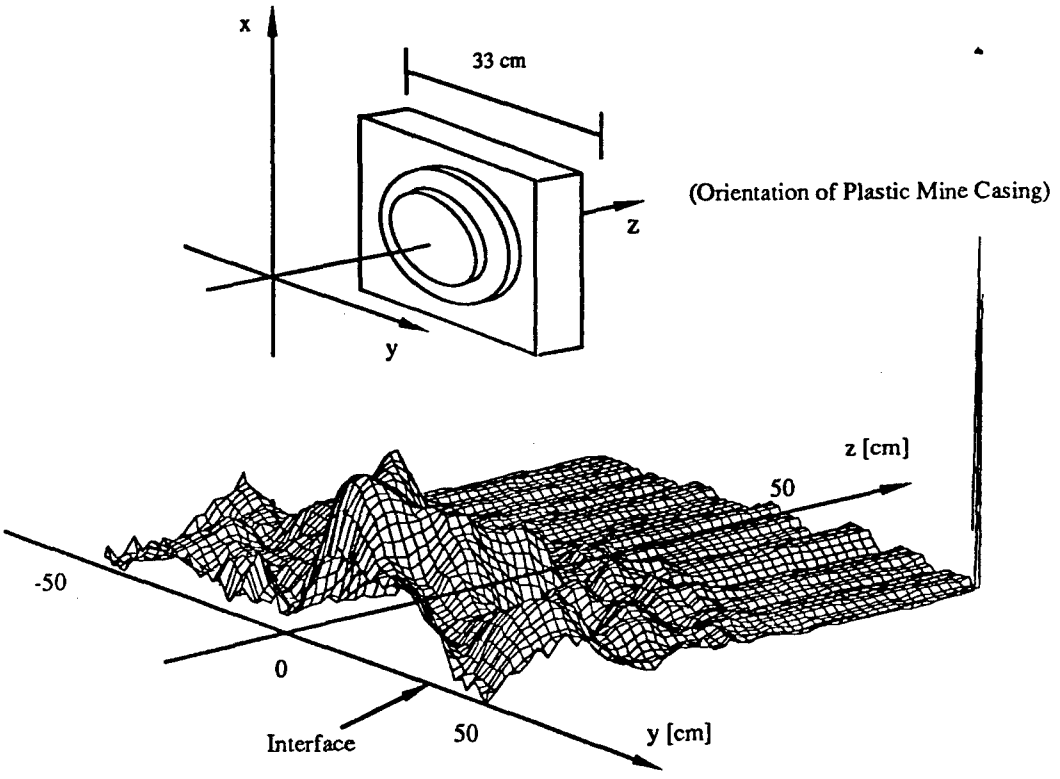

Figure 4 : Isometric Image of Plastic Mine 3" (7.5 cm) Below the Surface
ε_r = 5.5, σ = 0.145 Date: 08/01/90

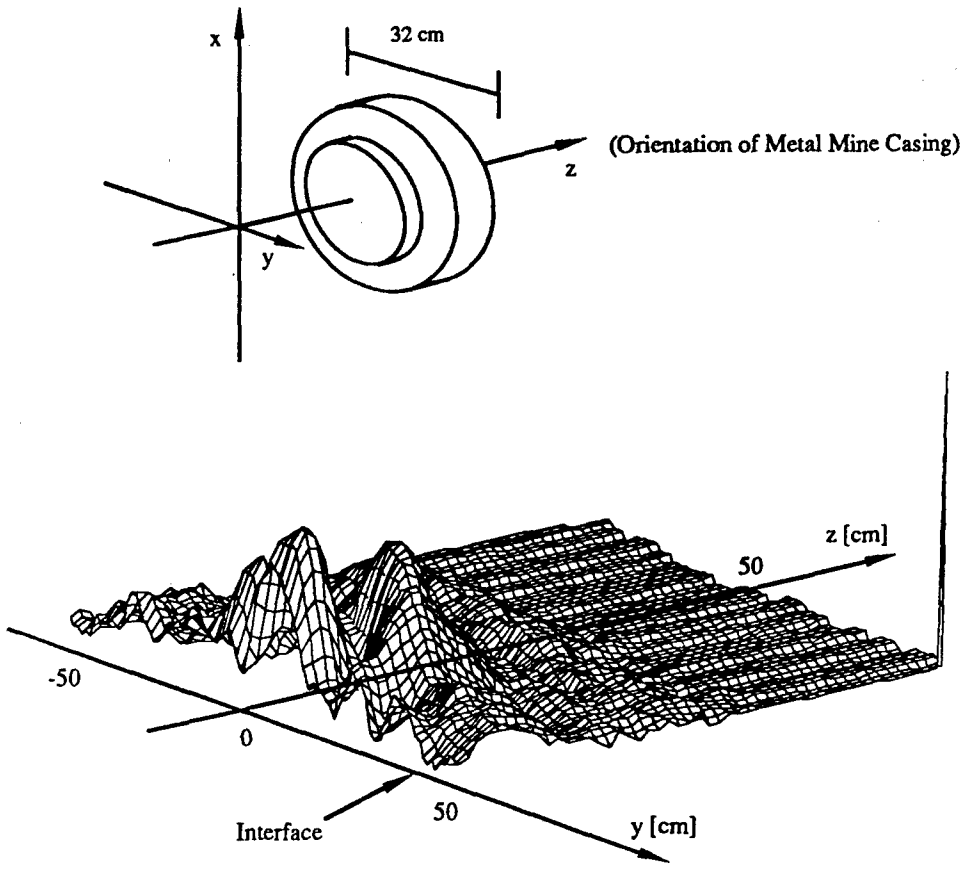

Figure 5 : Isometric Image of Metal Mine Casing 3" (7.5 cm) Below the Surface
ε_r =5.5, σ = 0.145 Date 08/29/90